Positron Emission Tomography/ Computed Tomography Imaging of Head and Neck Tumors: An Atlas

Michael M. Graham, MD, PhD, and Yusuf Menda, MD

The following images were all acquired using a CTI Bio-graph (Siemens Medical Solutions, Molecular Imaging Division, Hoffman Estates, IL) with 2-slice computed tomography (CT). Patients were injected intravenously with 10 to 15 mCi of ^{18}F-fluorodeoxyglucose (FDG) and imaged beginning 90 minutes ($\pm$10) later at 5 minutes per bed position. Most patients were sedated with 0.5 to 1 mg of alprazolam given orally 20 to 30 minutes before injection of FDG. Images were reconstructed with an OSEM iterative algorithm (5-mm FWHM). Slice thickness was 3.4 mm. The images were re-constructed with 3.5-mm pixels, interpolated to smaller pixels in magnified images. All images shown are magnified and brightened to best illustrate the important findings. Each image set includes FDG-positron emission tomography (PET) images, coregistered CT images, and fused PET-CT images in coronal, sagittal, and transaxial imaging planes.

The images were selected from approximately 1500 studies of patients with head and neck pathology studied from August 2003 to February 2005. The selected images show the most common tumors seen in the head and neck. We purposely did not select large tumors, which can be easily seen and defined. The goal is to illustrate the common findings seen in FDG PET-CT imaging of tumors in the head and neck.

Department of Radiology, University of Iowa, Iowa City, IA.
Address reprint requests to Michael M. Graham, MD, PhD, Department of Radiology, 3863 JPP, University of Iowa, 200 Hawkins Drive, Iowa City, IA 52242. E-mail: Michael-graham@uiowa.edu
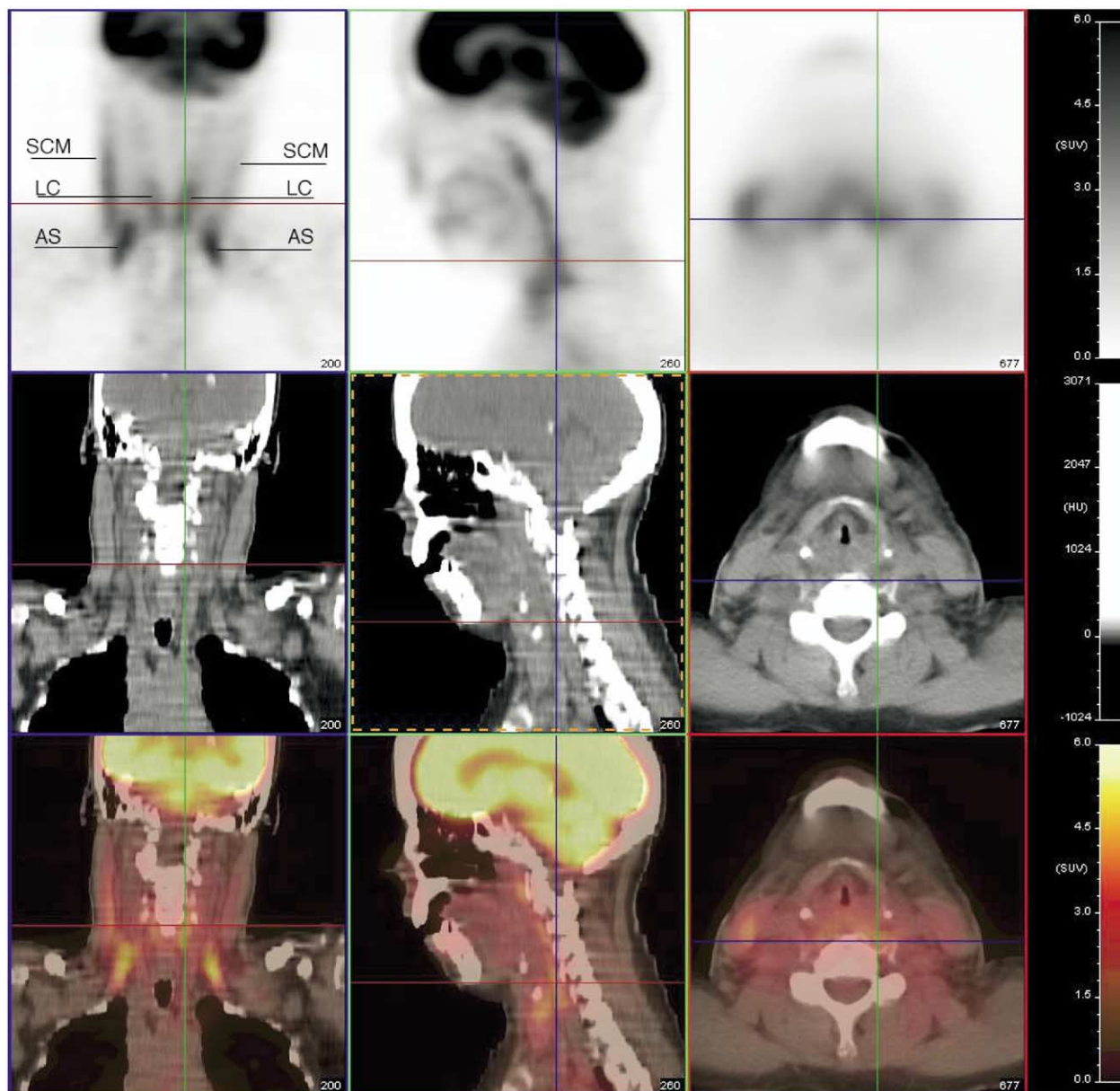
Appearance of Normal Structures

Figure 1 Normal uptake in sternocleidomastoid (SCM), longus coli (LC), and anterior scalene (AS) muscles. All these muscles are neck flexors but, in individual patients, uptake may be observed in one or more of these muscles. There also can be unilateral uptake as the result of torsion of the neck or irritation of the nerves innervating specific muscles. The crosshairs are on the left longus coli muscle. The sagittal images show the length of the muscle as it extends superiorly in the prevertebral space. In general, during the uptake period, patients should be in a neutral, relatively uninteresting environment to minimize muscular activity.
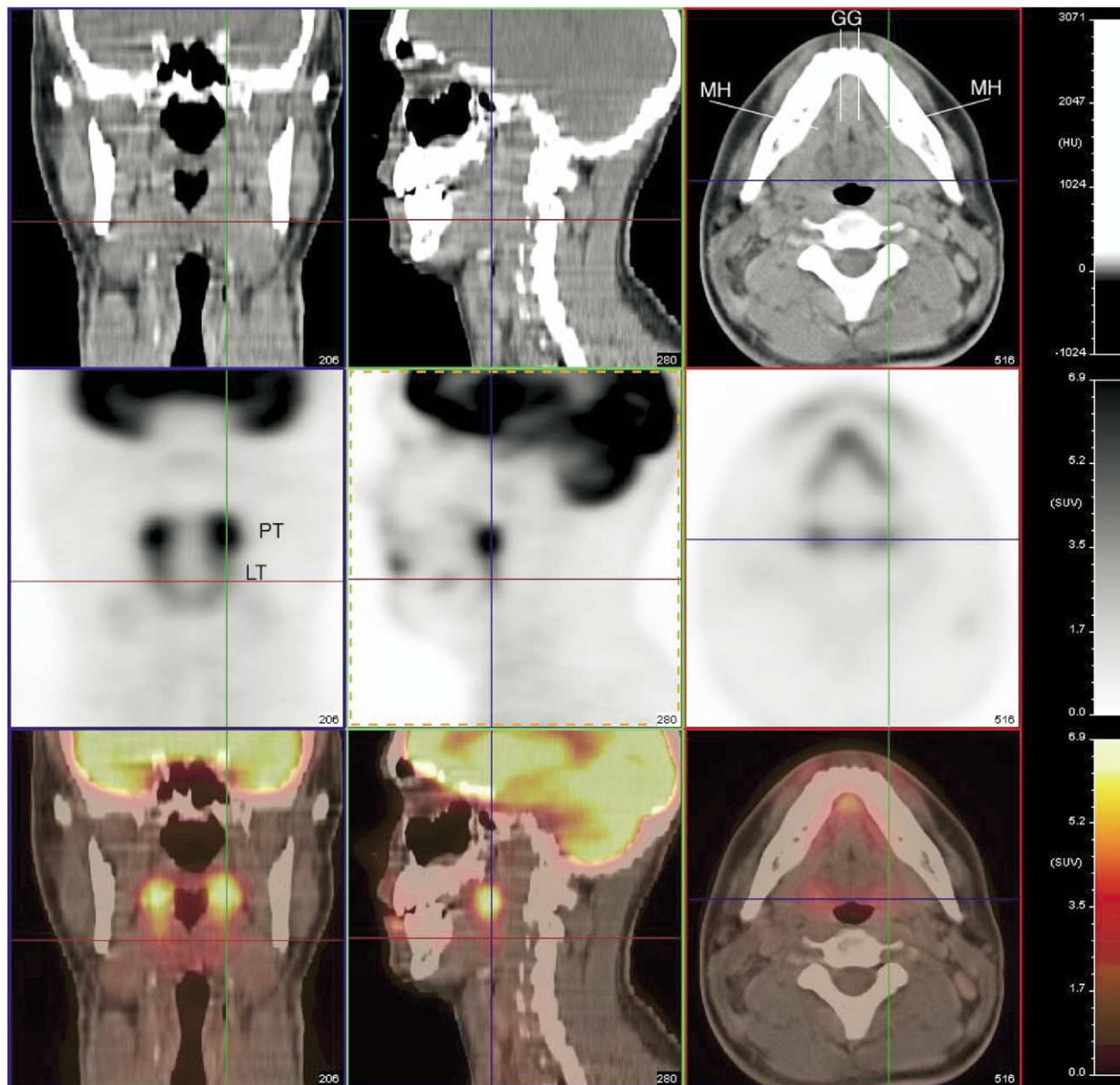
Figure 2 Normal uptake in the palatine (PT) and lingual (LT) tonsils and in the myelohyoid (MH) muscle immediately posterior to the mandible. The myelohyoid uptake is combined with sublingual salivary gland uptake because these glands are located immediately inferior to the myelohyoid muscles. The medial tongue muscles are the genioglossus (GG) muscles. Uptake in these structures is variable but is almost always symmetric. In this subject, the uptake in the palatine tonsils is greater than in the lingual tonsils.
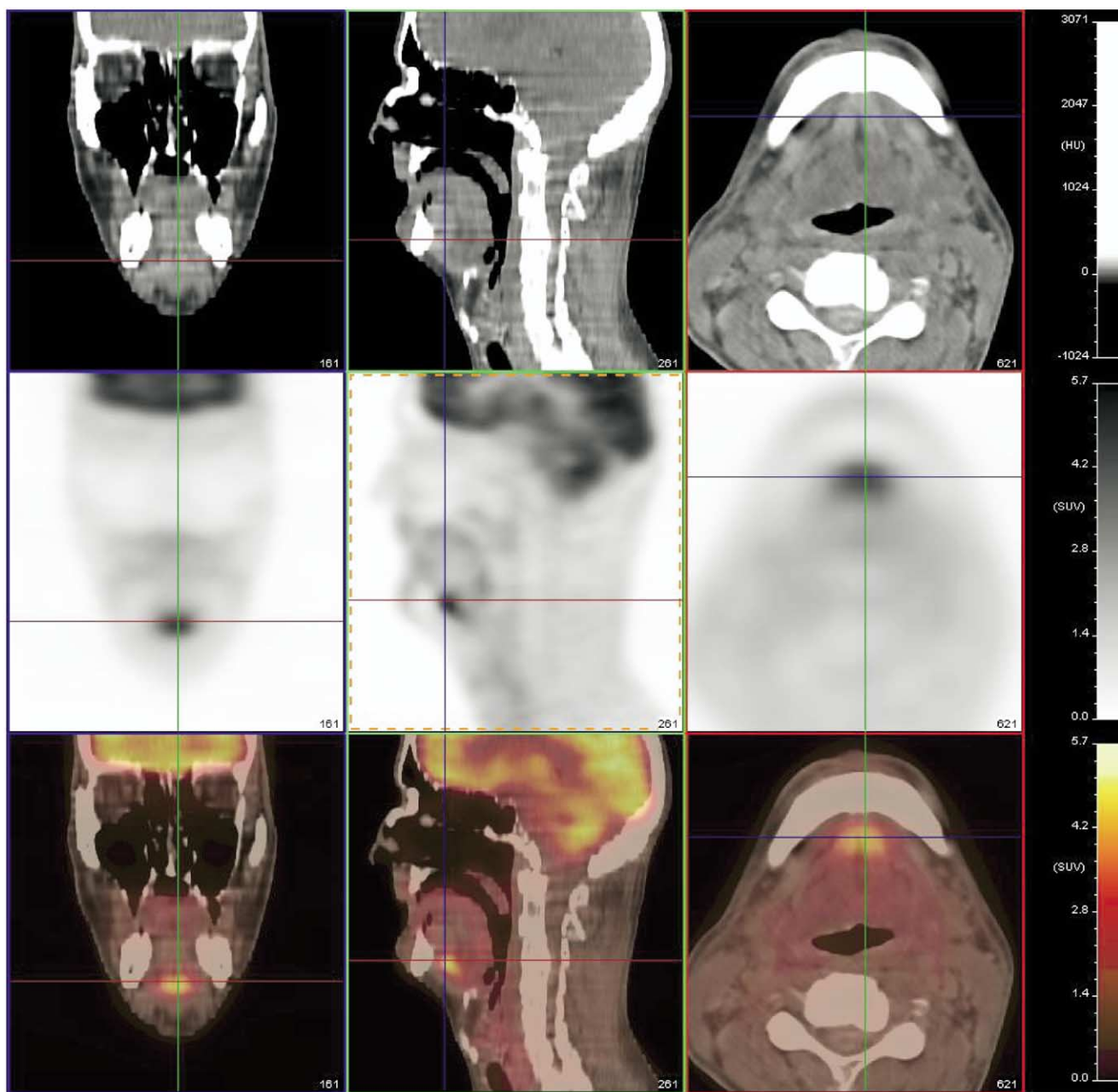
Figure 3 Normal uptake in the floor of the mouth, involving the anterior aspect of the genioglossus muscle, which is the paired muscle that looks like an upside-down V. Malignancies can occur in this region and usually can be identified by displacement of normal structures, such as the genioglossus muscle.
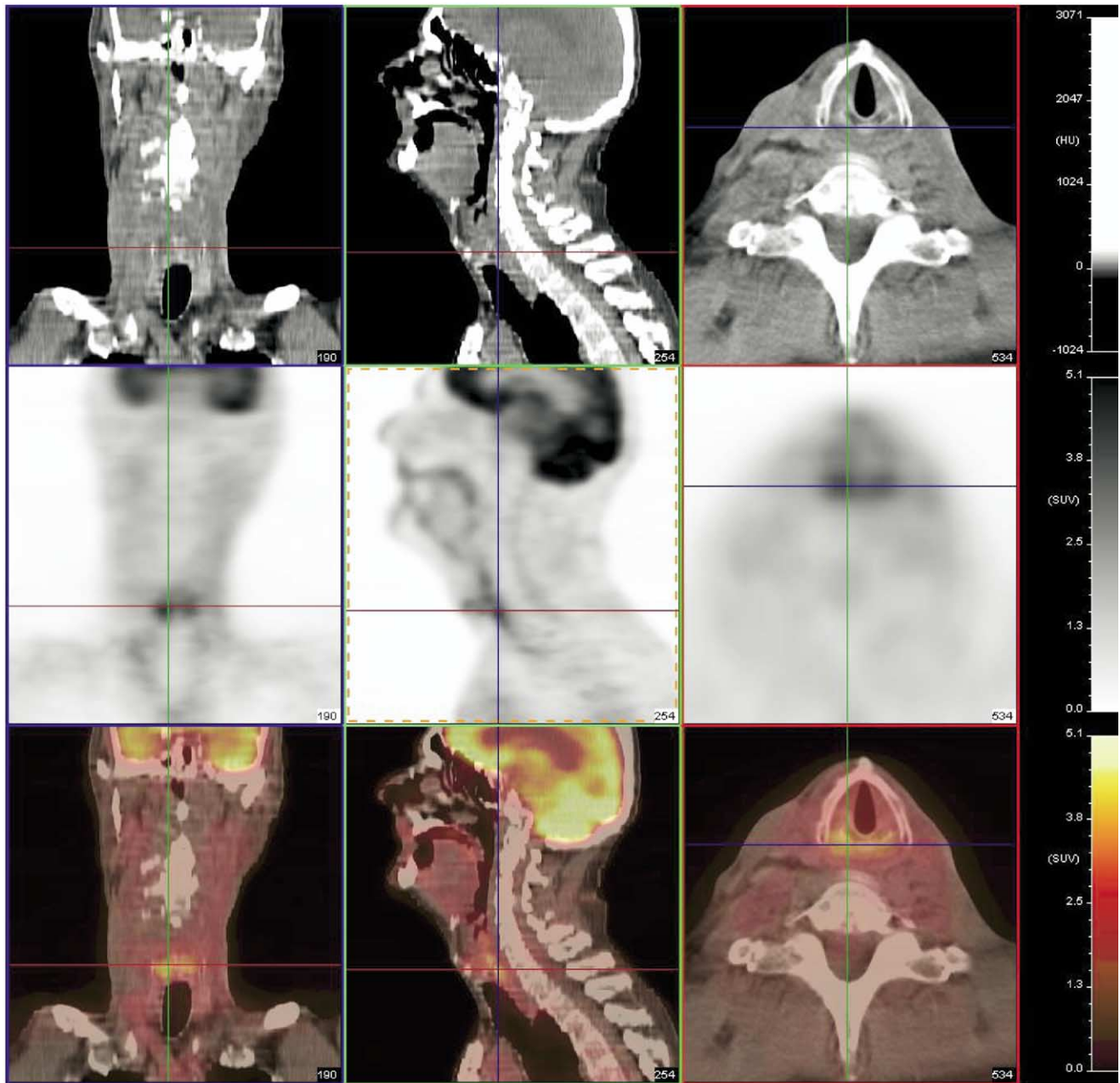
Figure 4 Normal uptake in the larynx, which occurs when patients use their voice during the uptake period. They should be instructed not to speak, sing, hum, or even subvocalize during the uptake period. Uptake associated with speech is almost always symmetric and usually is most intense in the area of the arytenoid cartilages, as seen in this subject. The vocal cords attach to the arytenoid cartilage anteriorly and several muscles attach posteriorly. These posterior muscles (thyroarytenoid and cricoarytenoid muscles) are the sites of increased uptake. The arytenoid cartilages commonly calcify in adults and are visible as sites of increased density on the CT images.
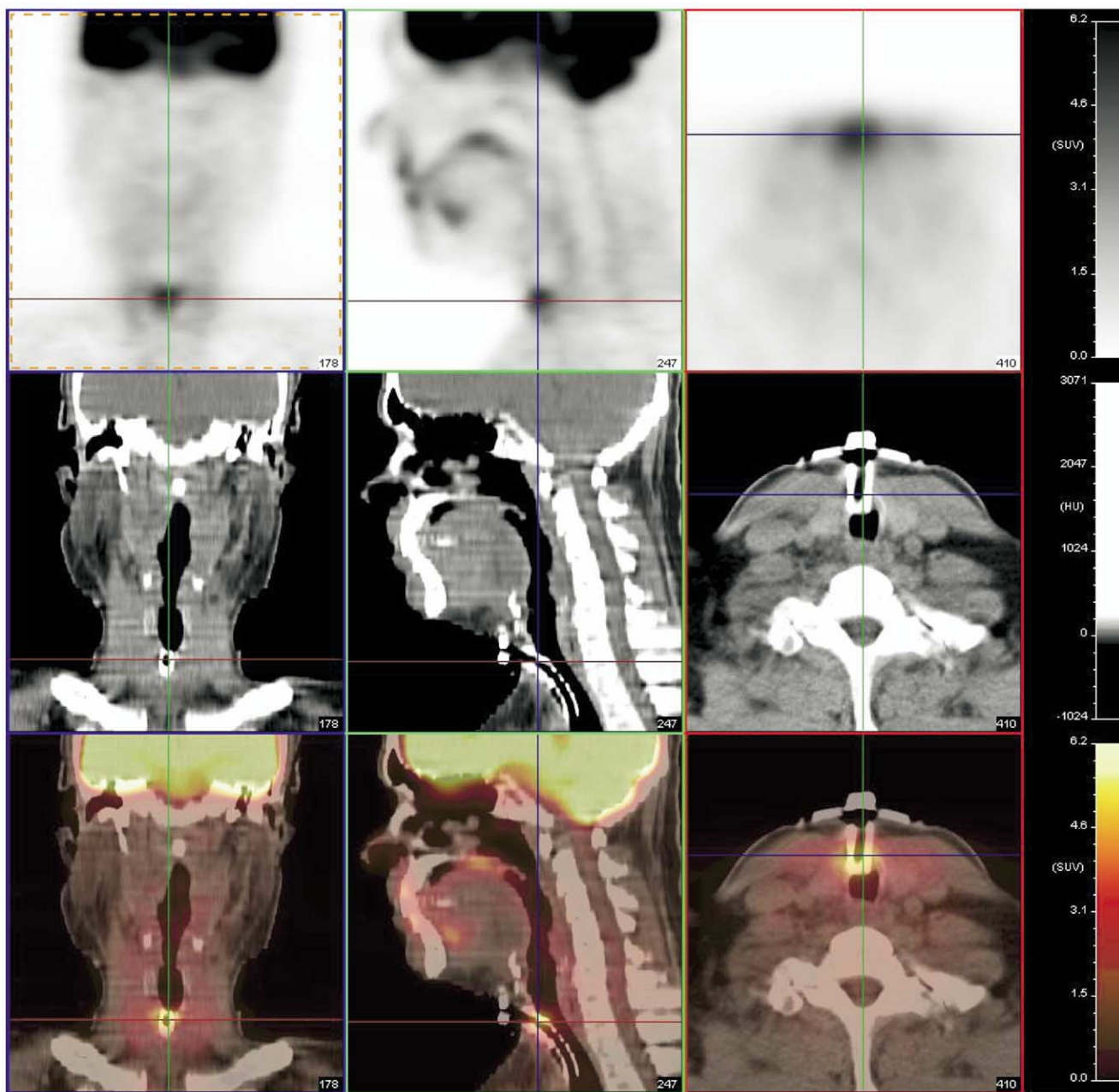
Figure 5 Normal uptake in a tracheostomy site. These sites often have granulation tissue that shows moderately increased uptake of FDG. Uptake is usually symmetric. Asymmetric, more intense uptake, can be seen with recurrent disease and should be biopsied.
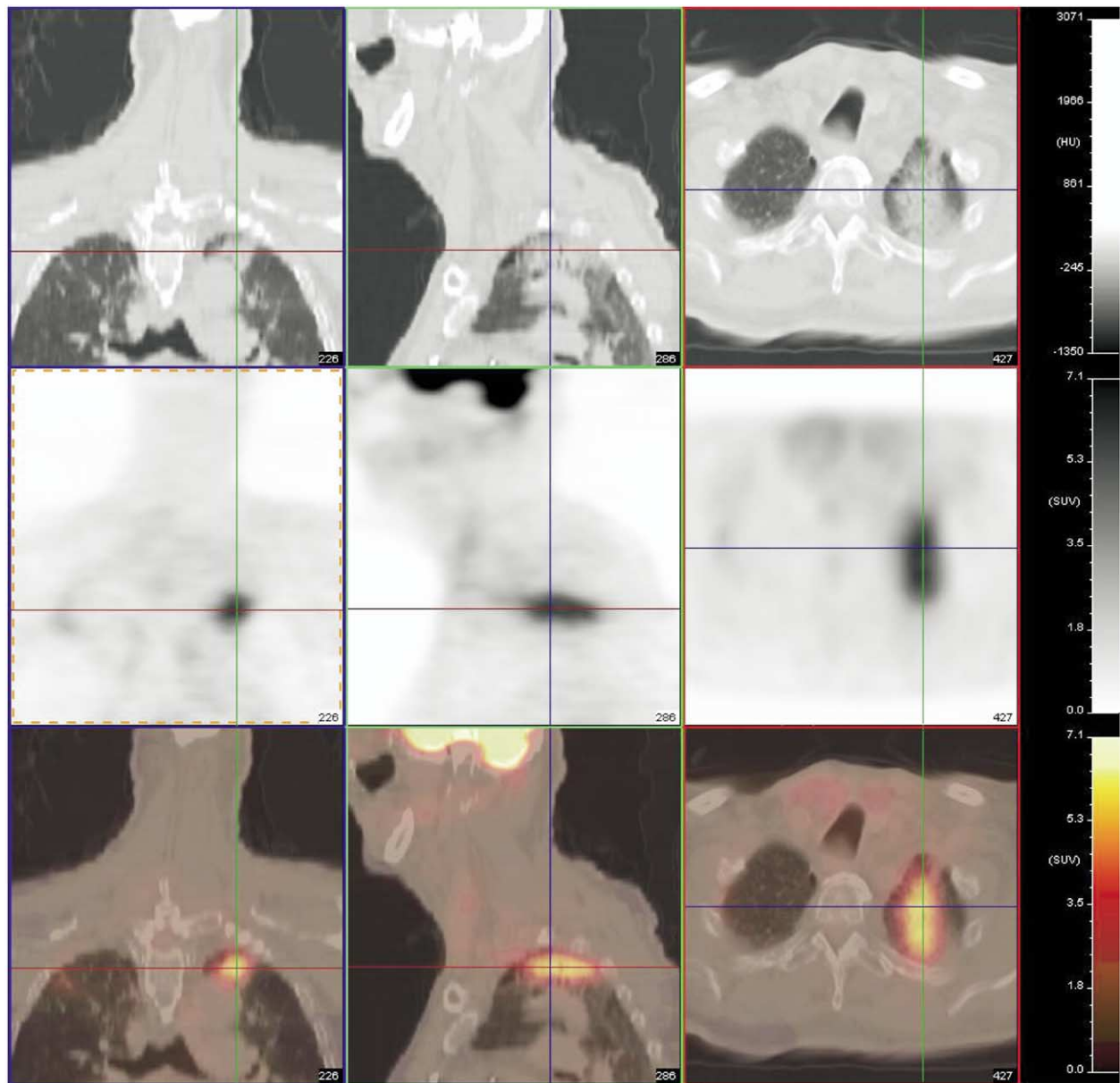
Figure 6 Uptake in radiation fibrosis of the lung. This patient had carcinoma of the larynx treated with radiation, which ended 8 weeks before the PET study. When head and neck cancer patients are treated with radiotherapy, it is quite common to include the apices of the lungs in the treatment ports. Such irradiated lung will develop an inflammatory response that progresses to fibrosis. During the inflammatory phase, which lasts for approximately 3 months after radiotherapy, it is common to see moderate uptake with FDG. An important clue that this uptake is caused by radiation is the linear shape of the uptake in the lung, as well as its apical location.
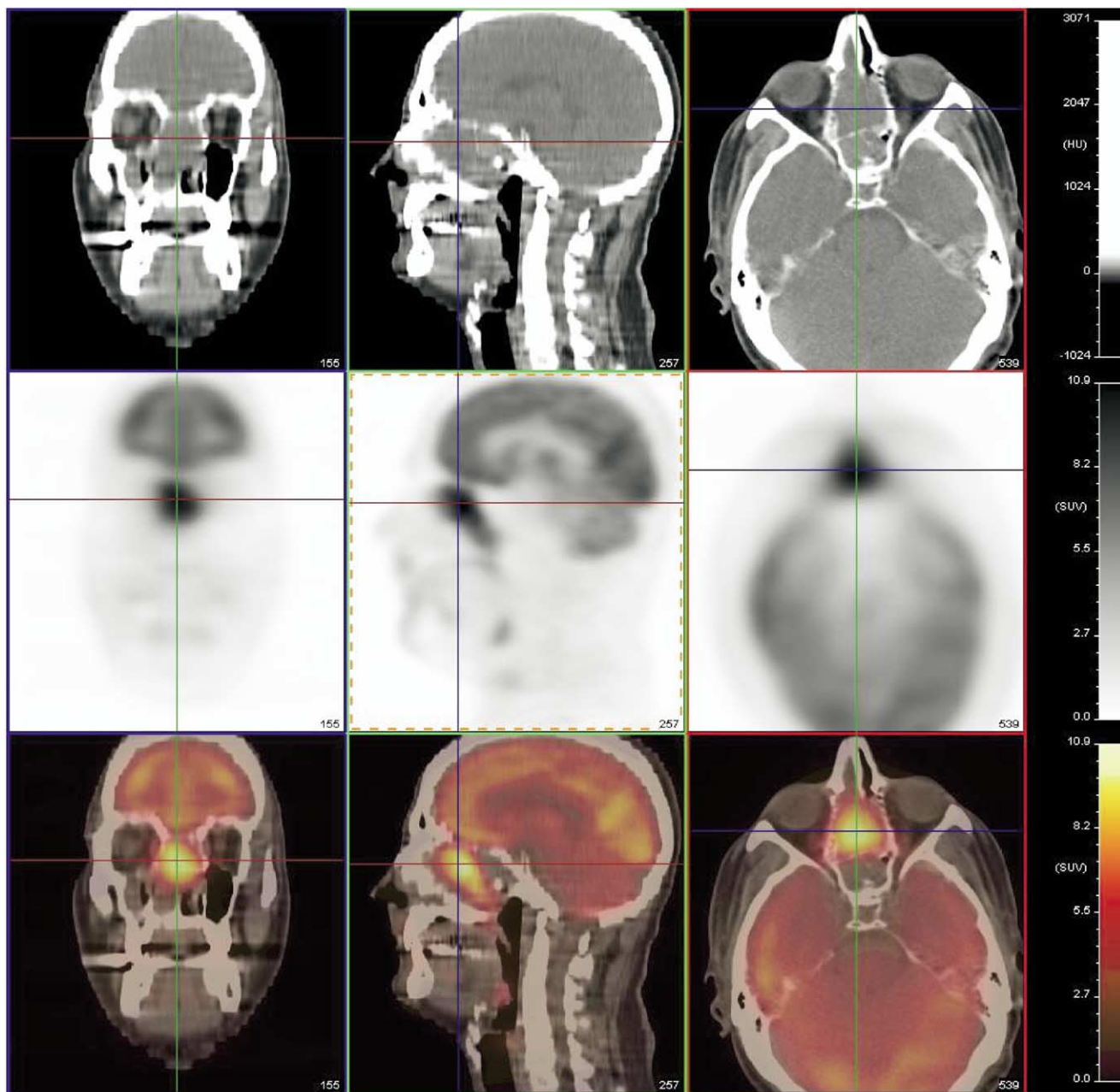
Sino-Nasal Malignancies

Figure 7 A poorly differentiated squamous cell carcinoma of the ethmoid sinuses. The images show metabolically active tumor filling the ethmoid sinuses, which are usually filled with air. Most patients with tumors of the paranasal sinuses present with advanced disease, and cure rates generally are poor. Squamous cell carcinoma is the most frequent type of malignant tumor of the paranasal sinuses. PET-CT imaging is most useful to define extent of disease, as a guide for the surgeon and radiotherapist. It is also useful for identifying metastatic disease, although these tumors usually do not metastasize.
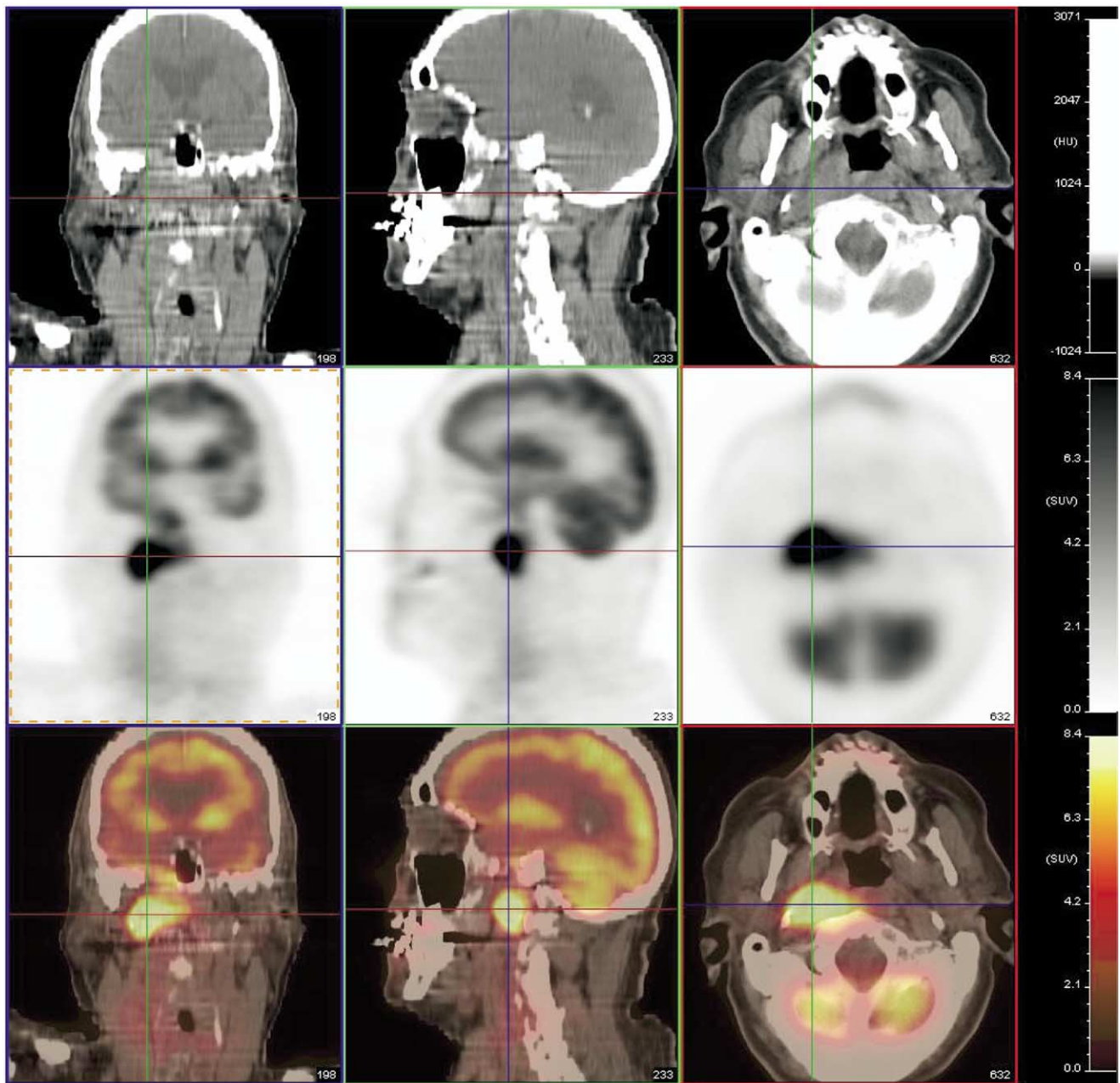
Figure 8 A right posterior nasopharyngeal squamous cell carcinoma. The nasopharynx is the upper part of the pharynx, above the soft palate. Early stage nasopharyngeal cancer, such as the one shown, usually are treated with radiotherapy. PET-CT imaging is used to identify any metastases and to define extent of disease to guide radiotherapy treatment planning.
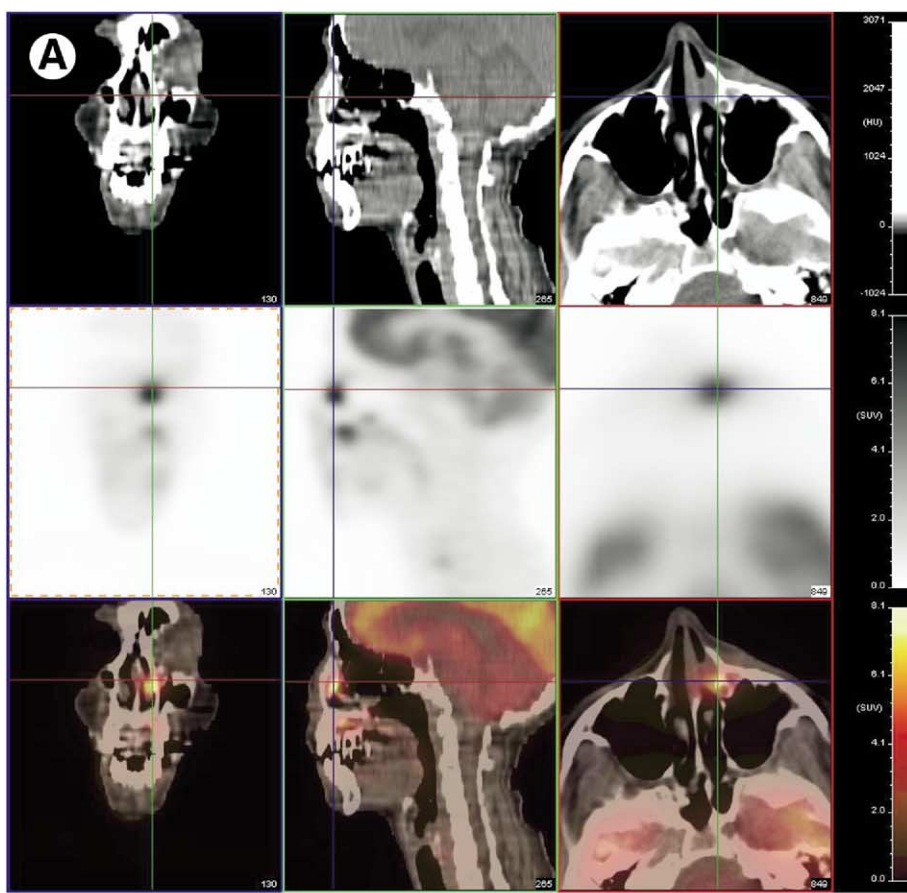
Figure 9 (A) Squamous cell carcinoma of the nasolacrimal duct. These cancers present relatively early because of obstruction of the lacrimal duct. Local metastases in the nasal cavity are relatively common and are very difficult to detect with CT or physical examination. PET-CT is probably the most sensitive way to detect these local metastases. (B) Two local metastases of the squamous cell carcinoma of the nasolacrimal duct shown in (A). The upper Figure shows one site in the lingual maxillary alveolus. The lower figure shows another site in the nasal mucosa. Neither site is identifiable by CT alone.
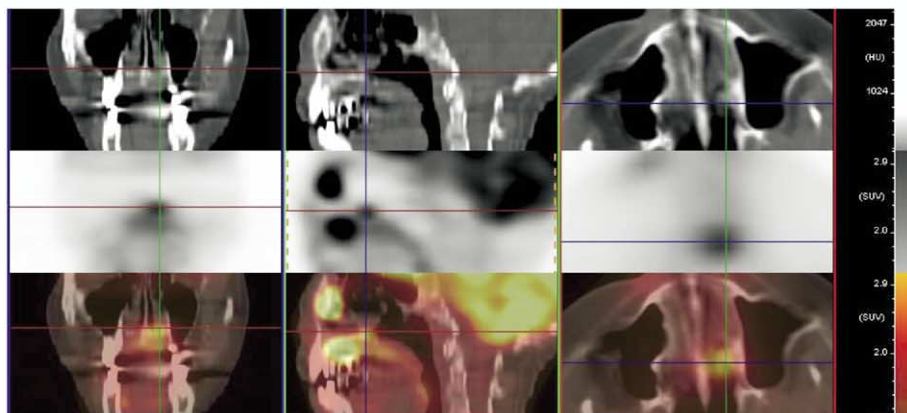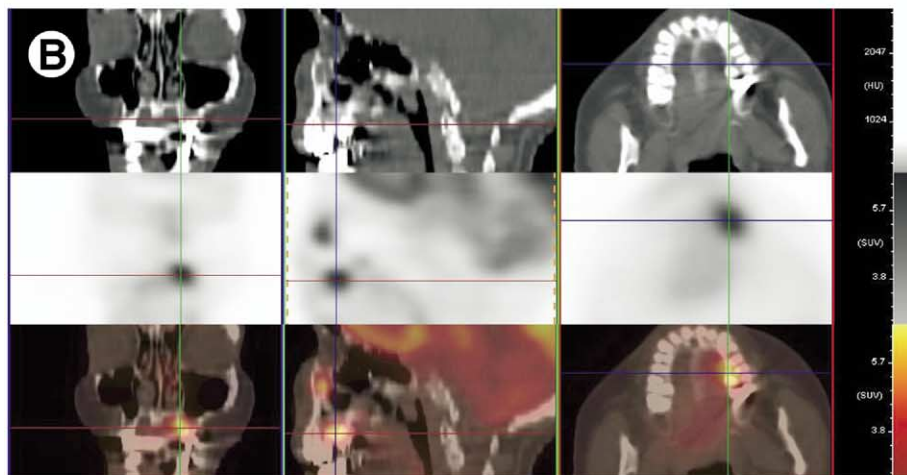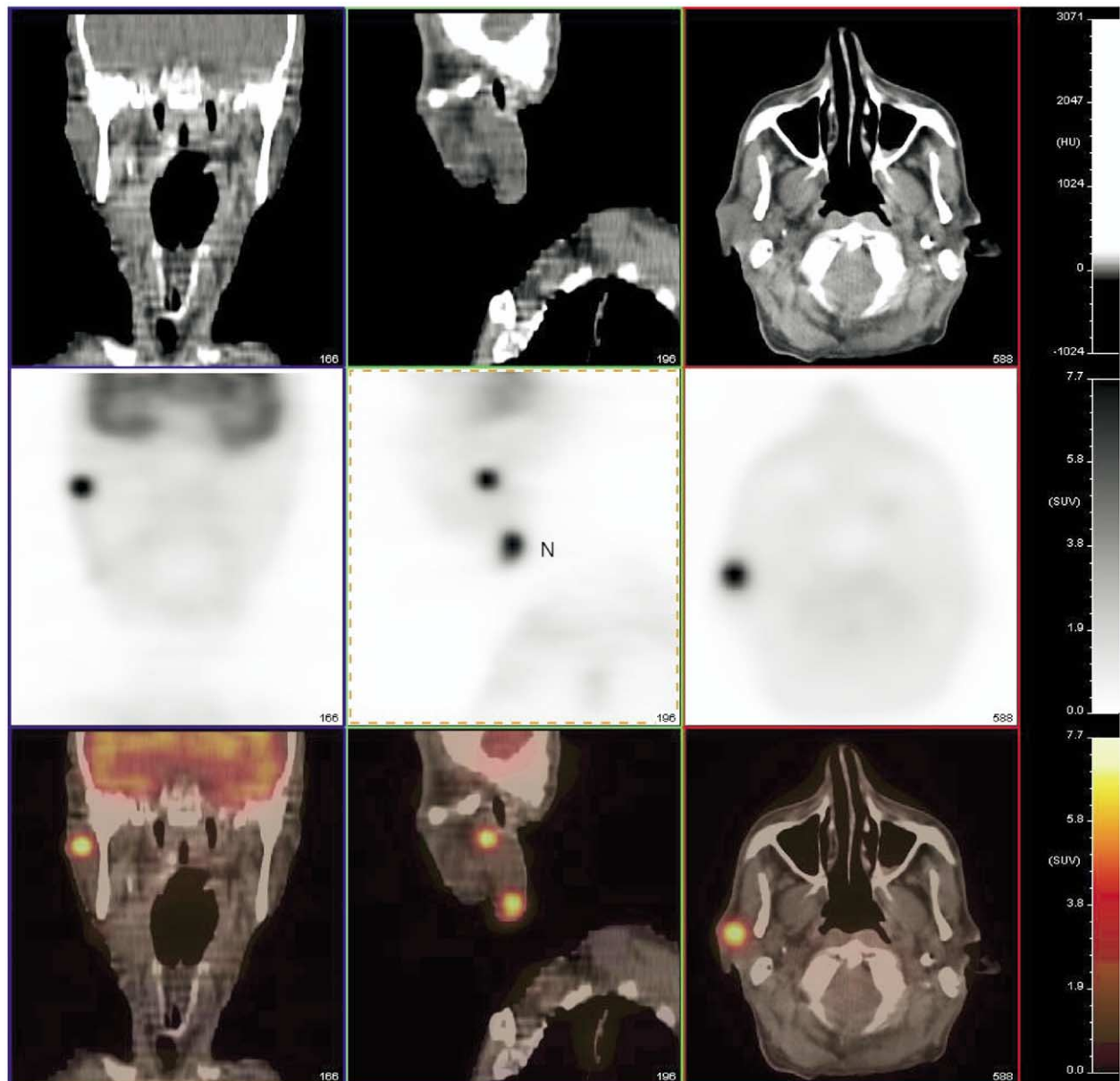
Salivary Gland Malignancies

Figure 10 A poorly differentiated carcinoma in the tail of the parotid salivary gland with metastasis to a level IIA lymph node (N). PET imaging is not as helpful in imaging salivary gland malignancies as compared with squamous cell carcinomas of the head and neck. This is because many benign tumors, such Warthin's tumor and pleomorphic adenomas, often show intense FDG uptake and some common salivary tumors such as acinar cell carcinoma often are not visualized with FDG.
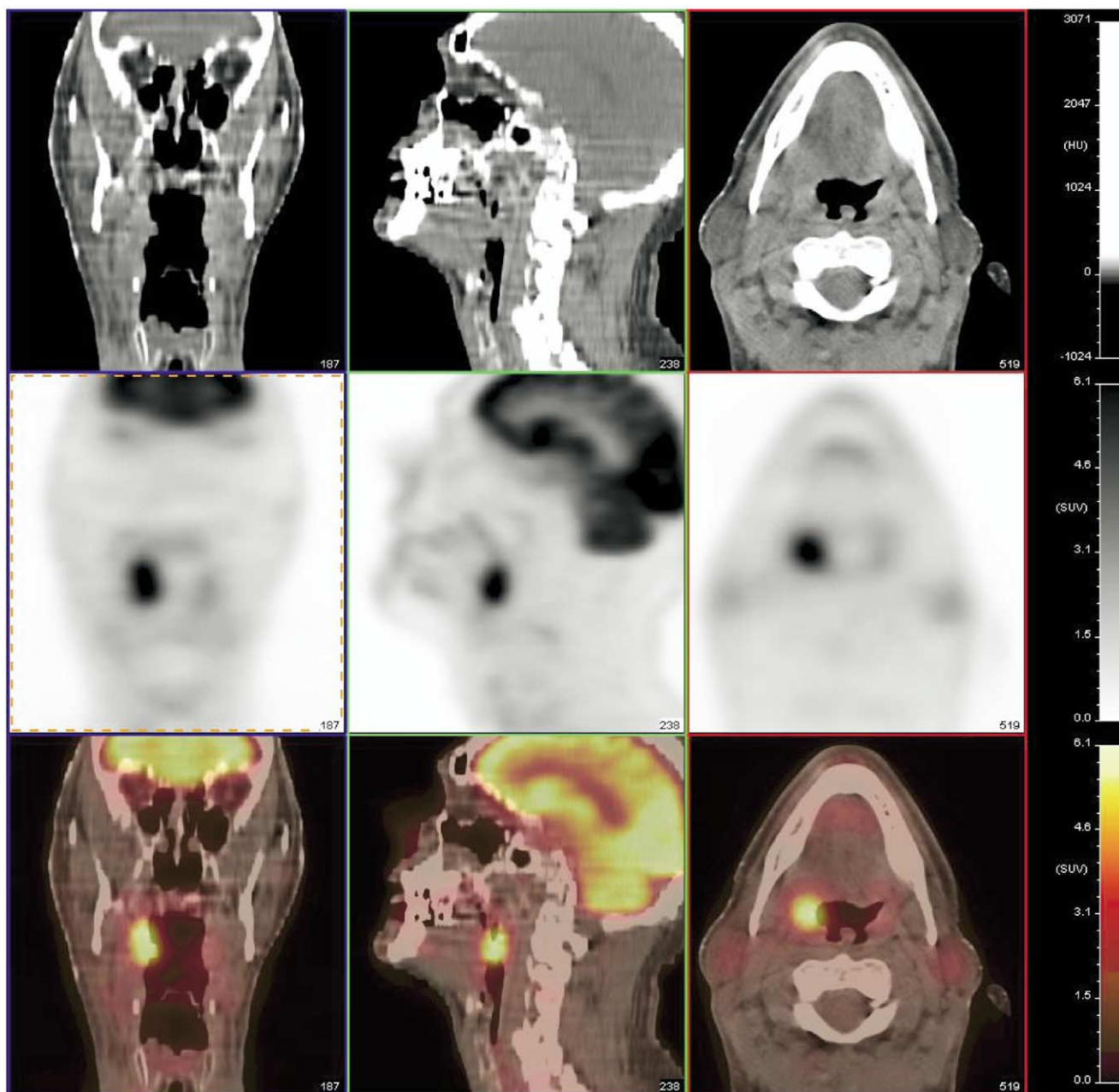
Squamous Cell Carcinoma of the Tonsils

Figure 11 Right tonsillar squamous cell carcinoma. It often is uncertain whether a tonsillar carcinoma arises in the lingual tonsil or palatine tonsil. In reality, these carcinomas frequently arise in the anterior tonsillar fold, which is probably where this carcinoma arose. Tonsillar carcinoma is the most common type of cancer in the neck. These tumors frequently metastasize to ipsilateral IIA lymph nodes. PET-CT imaging is worthwhile when there is clinical or CT evidence of metastatic disease. In this setting PET-CT often reveals additional disease, even occasionally contralateral, which changes management considerably. Currently, is does not seem to be worthwhile to do PET-CT imaging if there is no evidence of metastatic disease (ie, the N0 neck) because microscopic disease is frequently present and will not be detected by FDG-PET imaging.

Squamous Cell Carcinoma of the Oral Cavity (Tongue, Floor of Mouth, and Retromolar Trigone)
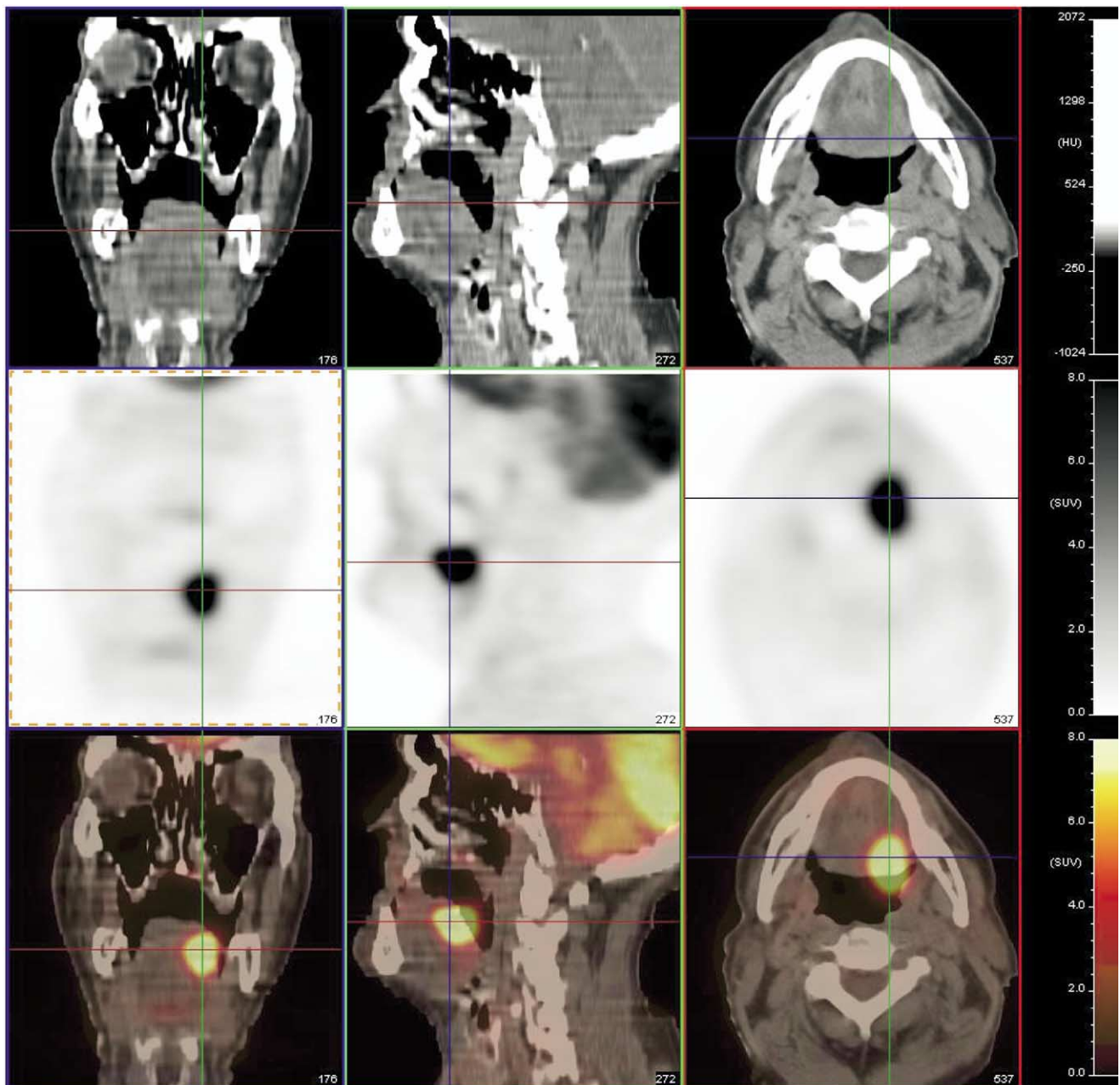

Figure 12 Squamous cell carcinoma involving the left oral tongue. The site of uptake is anterior to the lingual tonsil. Early carcinomas of the oral tongue can be difficult to detect with CT. As they enlarge, these tumors become more obvious because of displacement of normal structures.
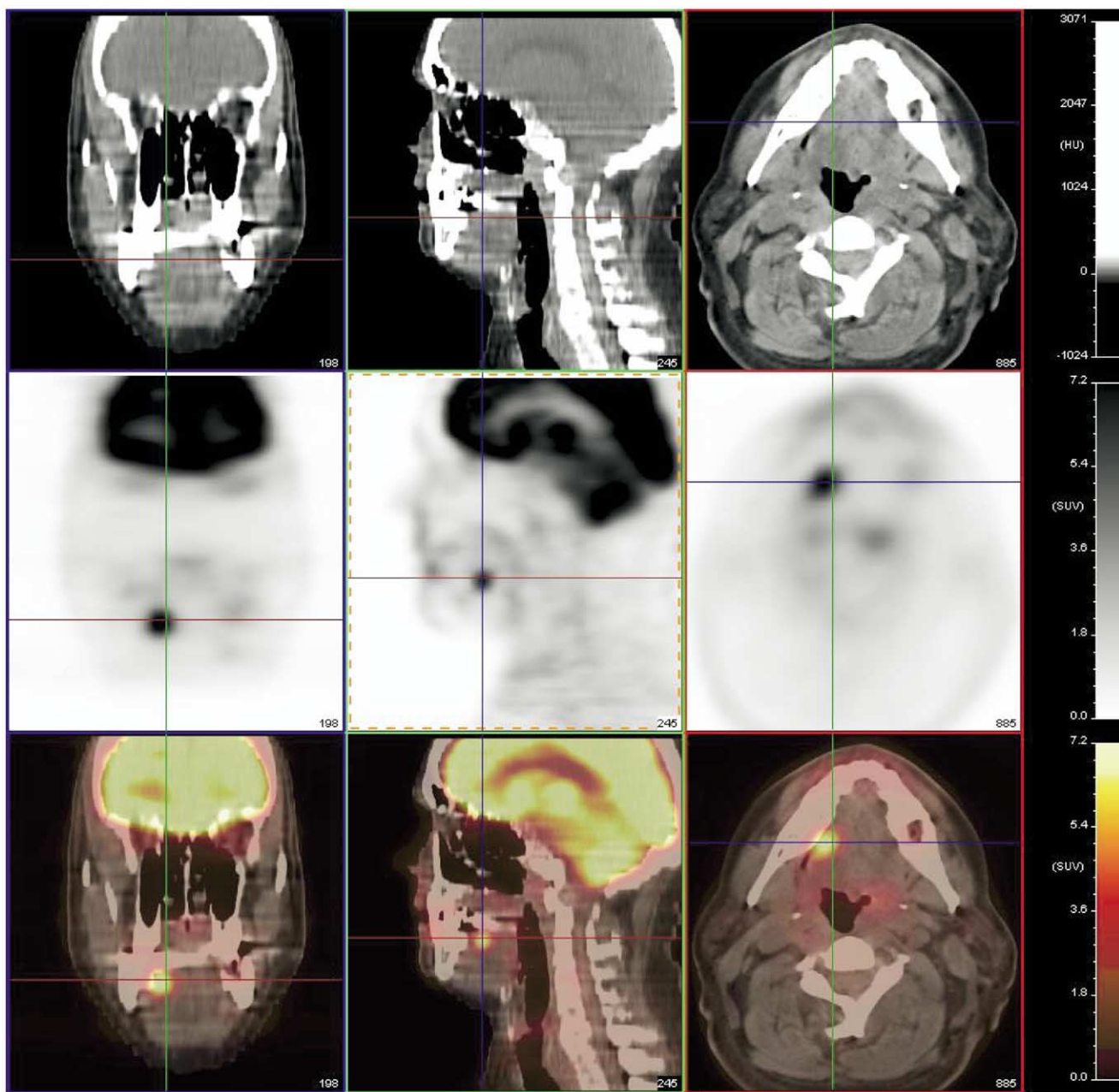
Figure 13 Squamous cell carcinoma involving the right lateral oral tongue. The 3 orthogonal views clearly show the focus of increased uptake is in the lateral tongue. This lesion is a T1 tumor (<2 cm).
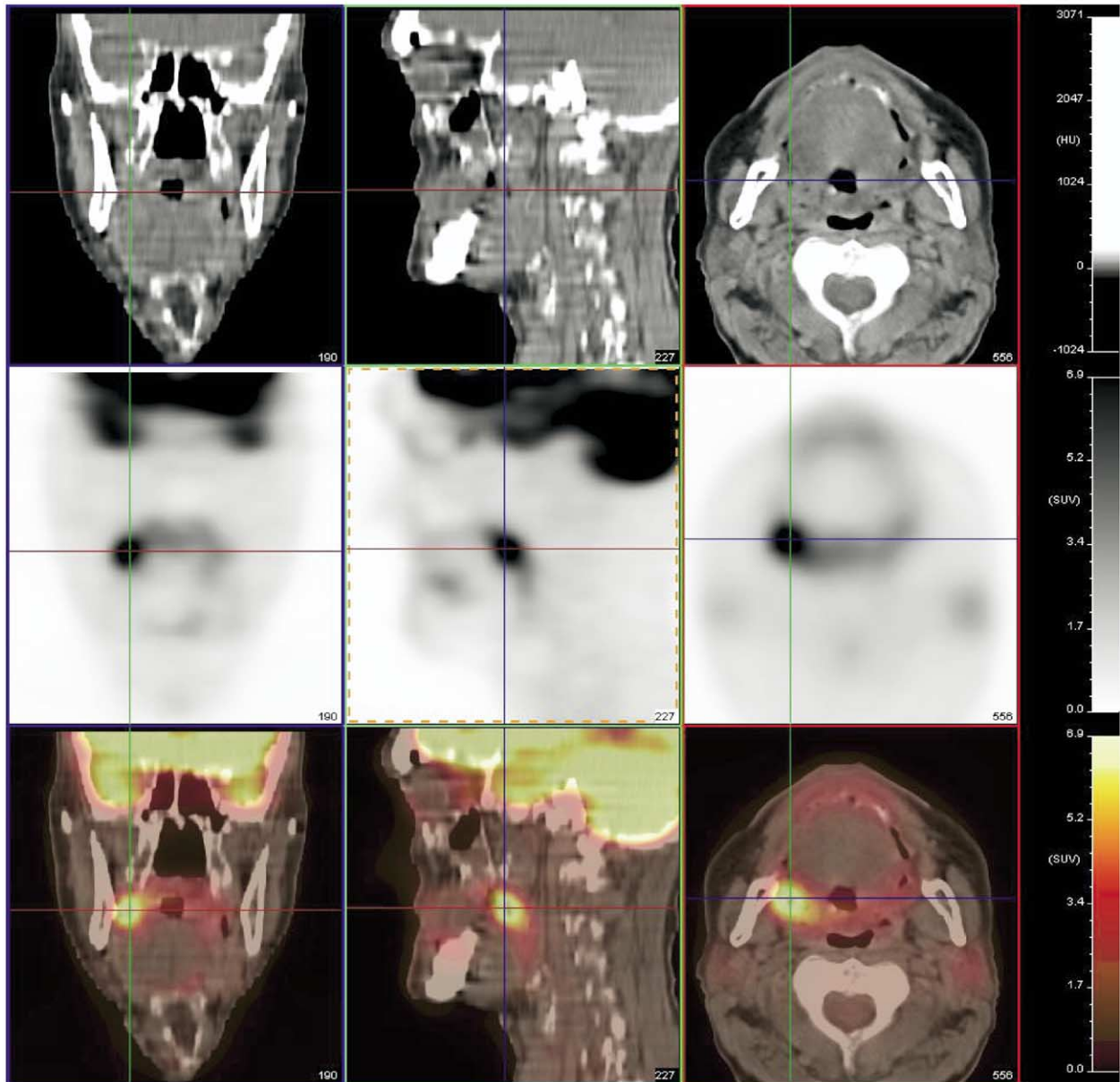
Figure 14 Squamous cell carcinoma of the retromolar trigone, the area immediately posterior to the third molar. This is a T2 lesion (between 2 and 4 cm). Retromolar trigone carcinomas frequently invade the mandible and the pterygoid or masseter muscles.
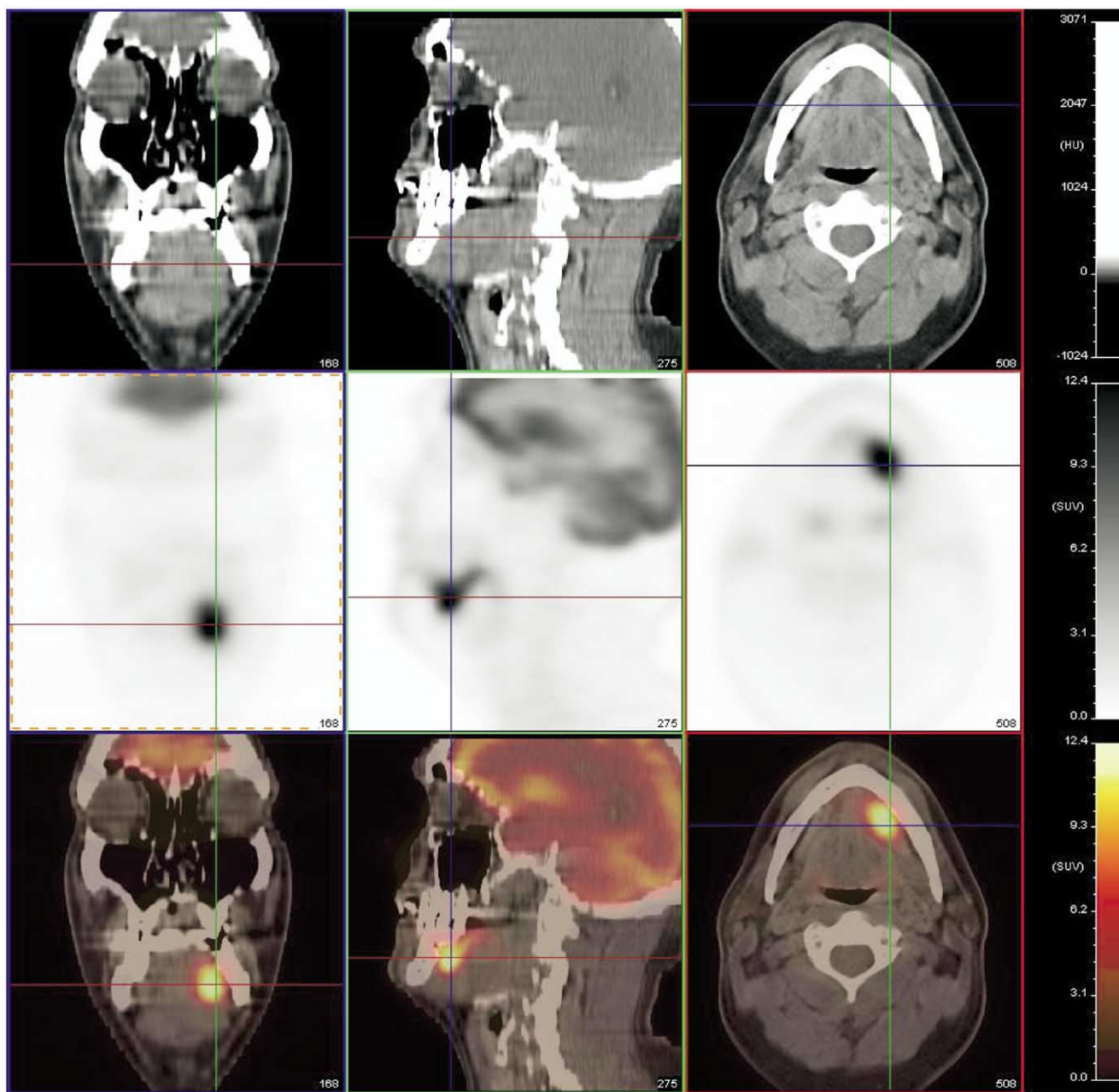
Figure 15 Squamous cell carcinoma of the left floor of the mouth, the region immediately inferior to the tongue. Cancer of the floor of the mouth accounts for about 30% of all oral cancers. This is a T2 lesion (between 2 and 4 cm).

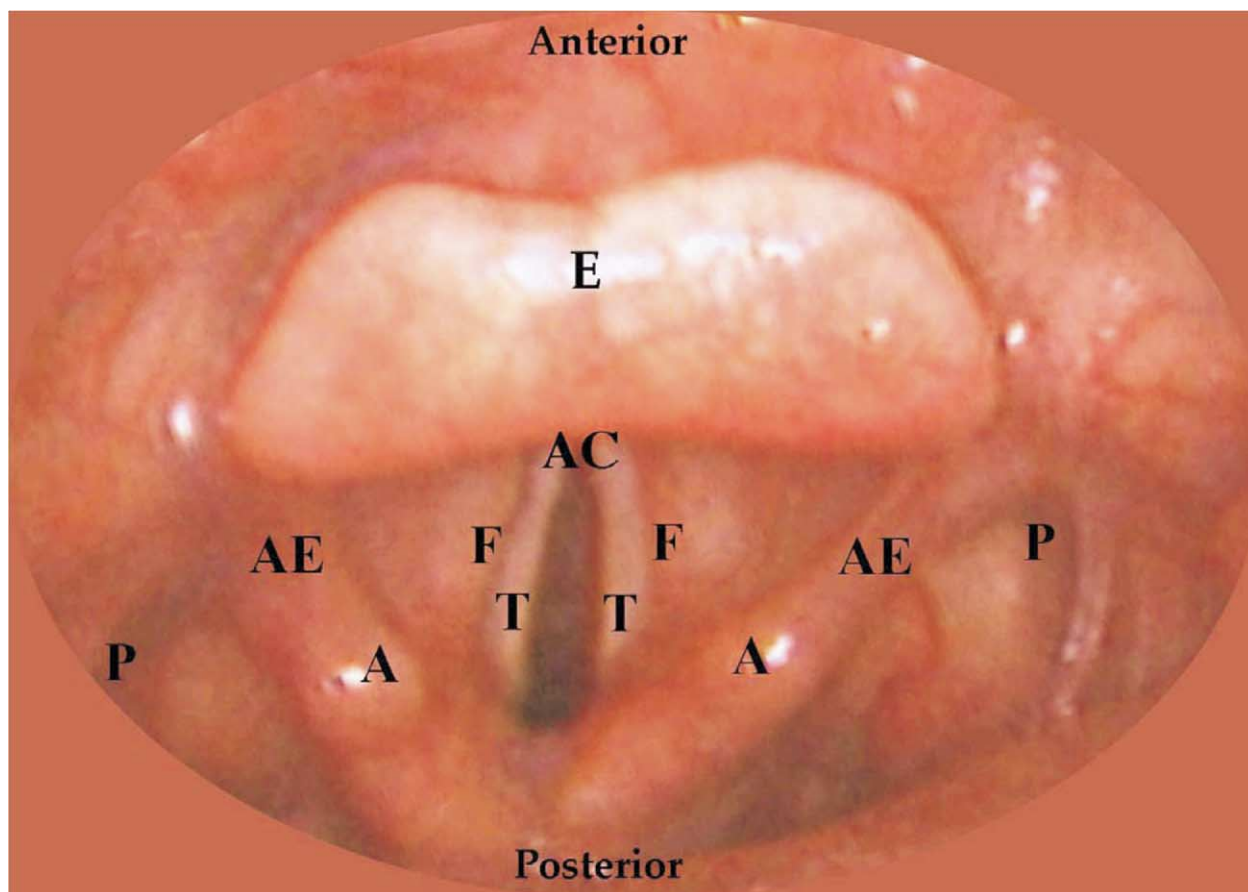# Anatomy of the Normal Larynx

Figure 16 The major relevant anatomic features of the larynx are shown: E, epiglottis; AC, anterior commissure; F, false vocal cord; T, true vocal cord; A, arytenoid cartilage; AE, aryepiglottic fold; P, piriform. sinus.

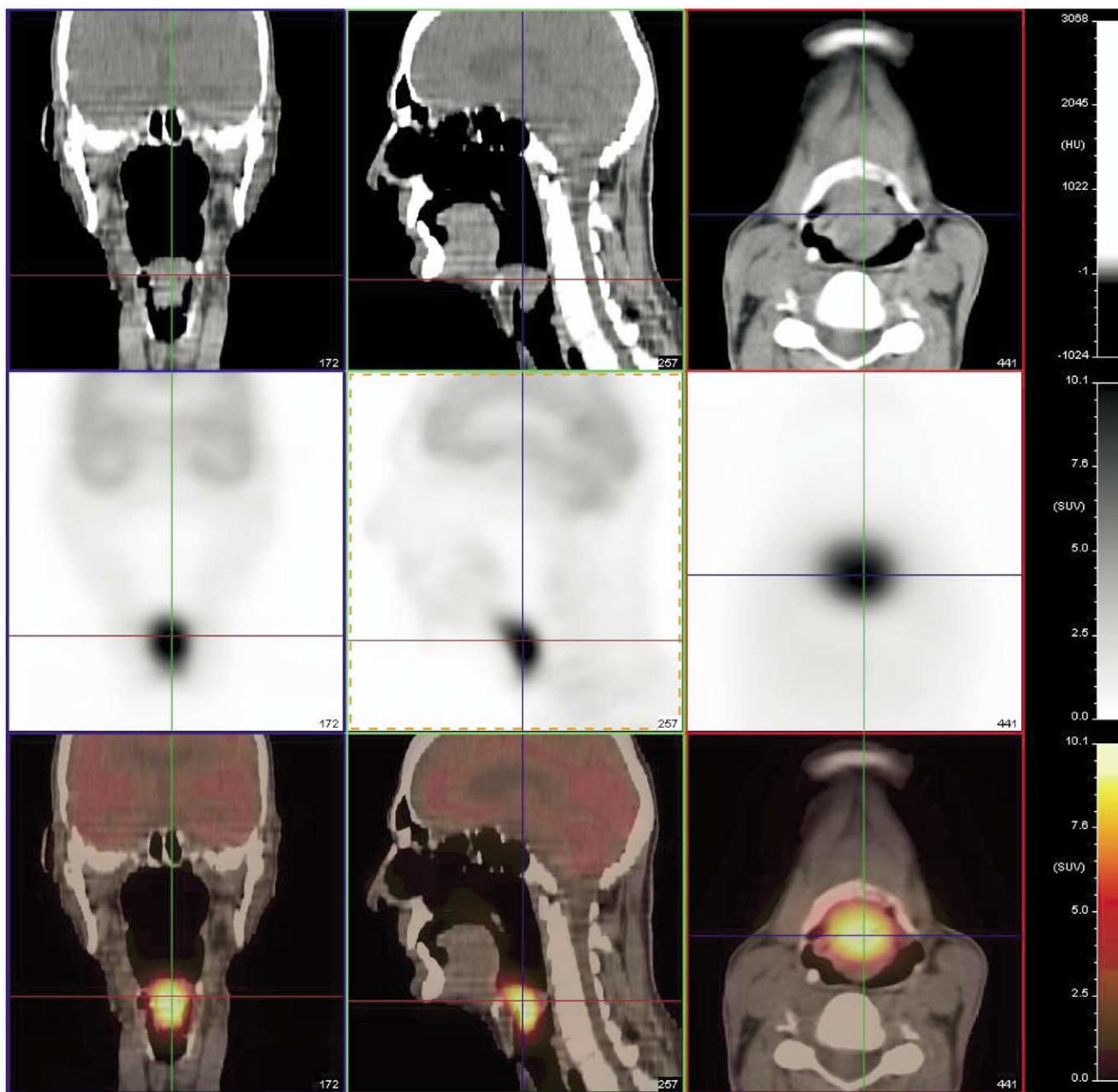# Squamous Cell Carcinoma of the Hypopharynx, Including Epiglottis, Piriform Sinus

Figure 17 Squamous cell carcinoma of the epiglottis. The epiglottis is in the midline superior to the larynx. This is a large tumor, which is threatening to obstruct the airway. These tumor often invade locally and it is important to carefully look for asymmetric extension of tumor.
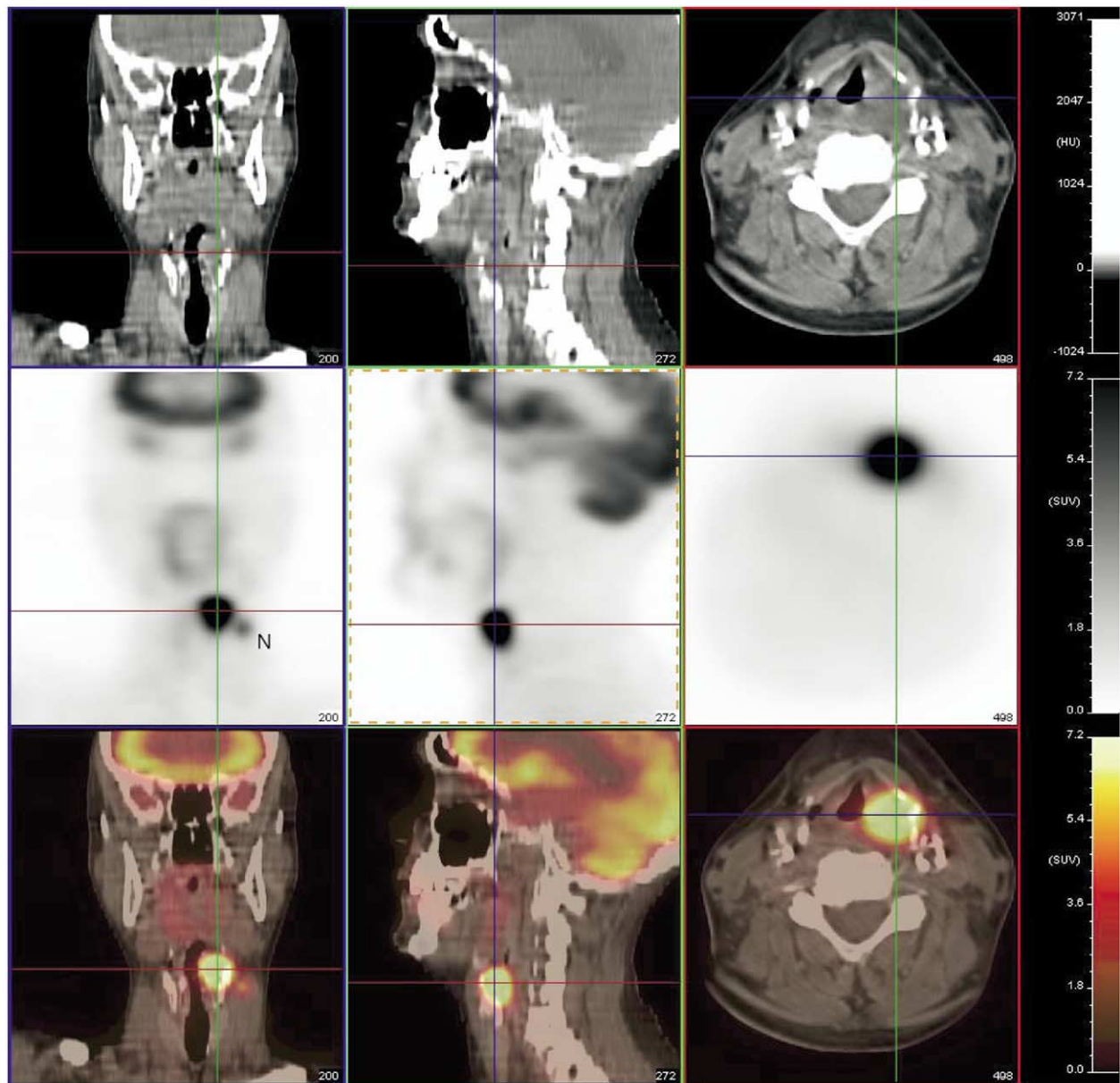
Figure 18 Squamous cell carcinoma of the left pirifom sinus (crosshairs). Metastatic disease in a nearby level III node (N) is seen in the coronal PET image. The tumor is displacing the larynx to the right. The piriform sinus is the most common site of malignancy in the hypopharynx. Piriform sinus cancers are extremely invasive with a high rate of metastasis to adjacent lymph nodes. Up to fifty percent of patients have positive nodes at the time of presentation.
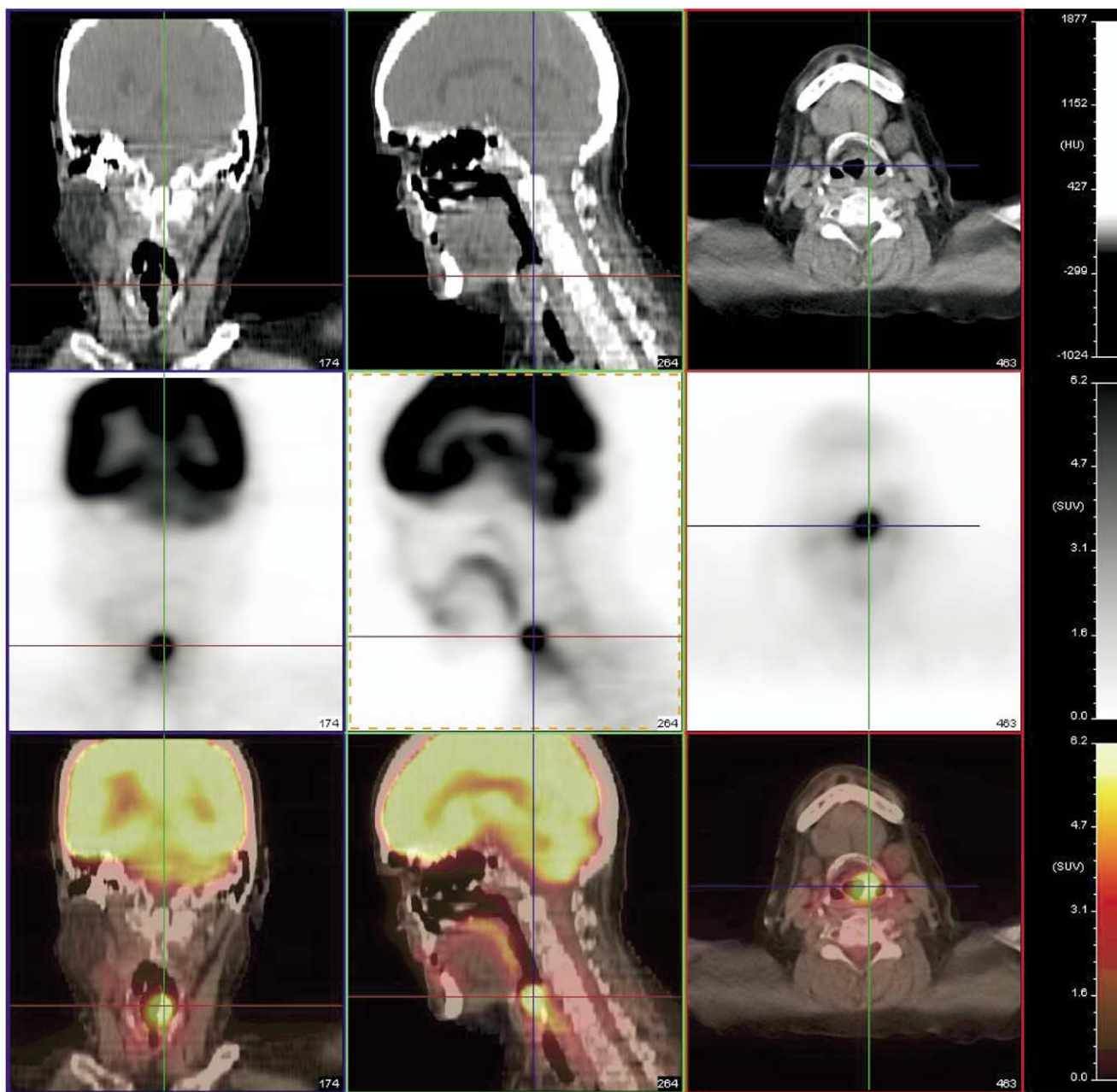
Figure 19 Squamous cell carcinoma of the left false cord extending into the aryepiglottic (AE) fold. The AE fold is thickened on the left. The bone immediately anterior to the AE fold is the hyoid, which can be distinguished from calcified thyroid cartilage by its rounded shape anteriorly. Thyroid cartilage is more pointed anteriorly. See Figures 20 and 21.
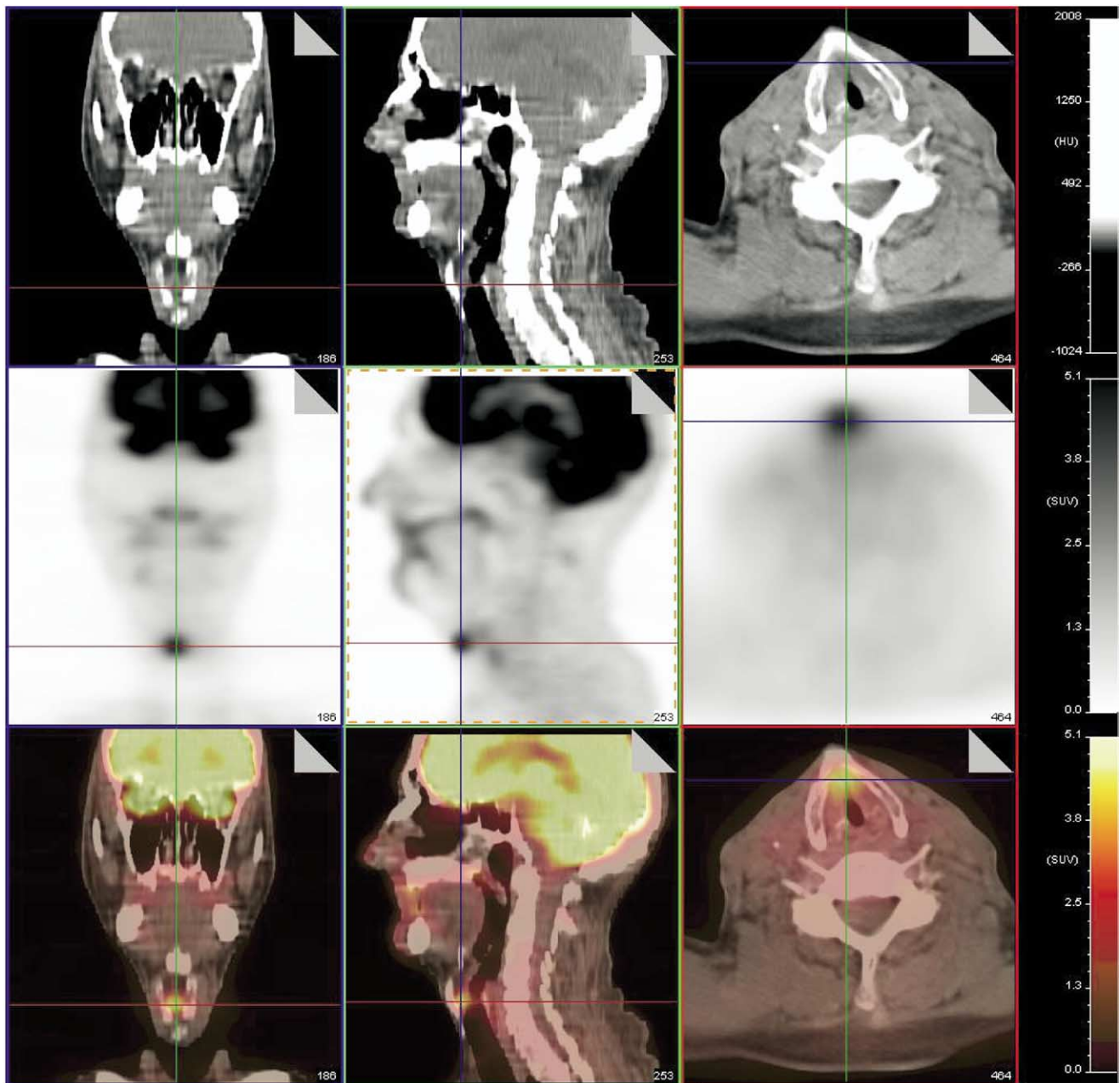
Squamous Cell Carcinoma of the Larynx

Figure 20 Squamous cell carcinoma of the anterior commissure of the larynx. The true vocal cords come together and attach to the thyroid cartilage at the anterior commissure. Laryngeal carcinoma can spread by direct extension both superiorly and inferiorly, as well as to local nodes. On CT it is important to look for invasion of the thyroid cartilage.
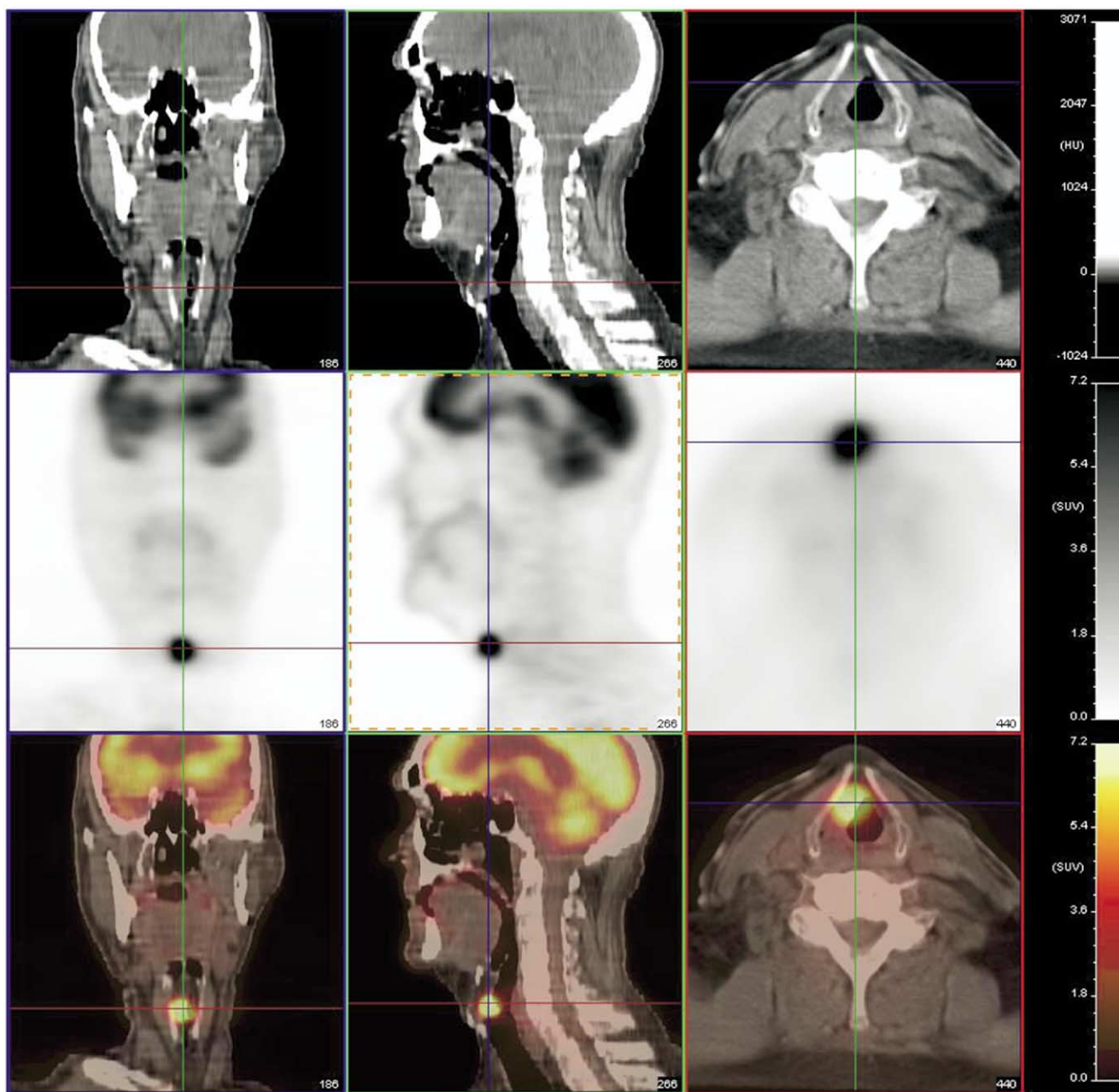
Figure 21 Squamous cell carcinoma of the false vocal cord. The thyroid cartilage is intact, so this is not a T4 lesion. It actually is a T3 lesion (limited to the larynx with vocal cord fixation). It is difficult or impossible to determine tumor stage by imaging, since vocal cord mobility is a major part of the staging criteria.

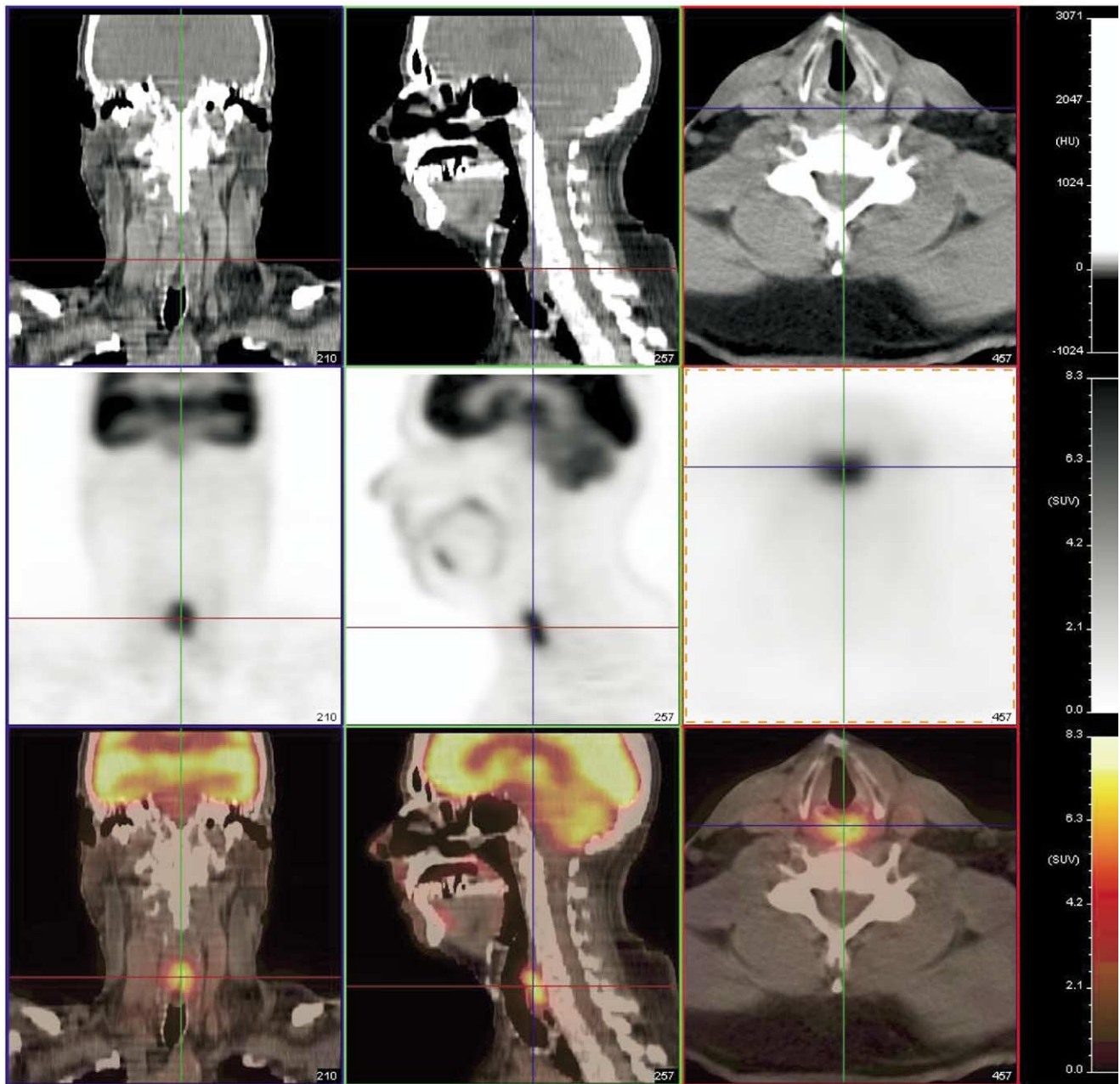# Squamous Cell Carcinoma of the Cervical Esophagus

Figure 22 Squamous cell carcinoma of the cervical esophagus that developed after radiotherapy for a previous laryngeal carcinoma. Secondary malignancies, although rare, can develop several years after radiotherapy. This focus of increased uptake can be localized to the esophagus by its posterior, midline location and its linear appearance in the sagittal images.
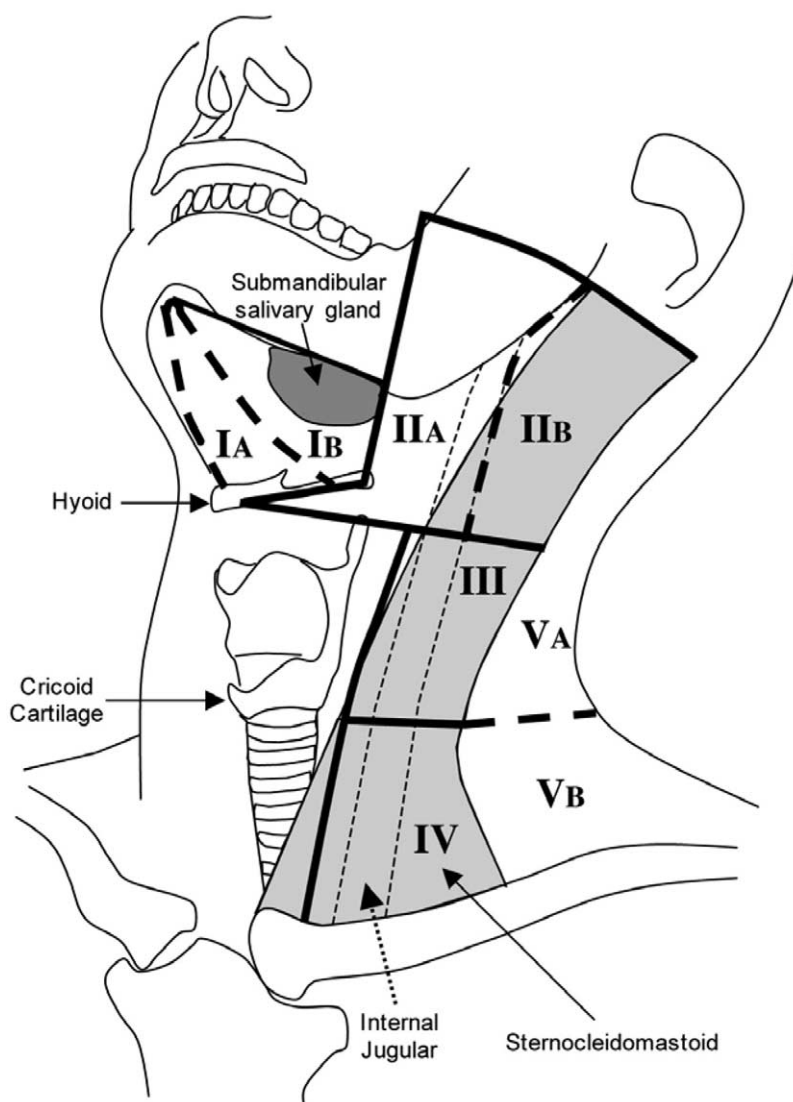
Nodal Levels in the Neck

Figure 23 Correct identification of nodal levels in the neck is important to achieve accurate communication with radiologists and head and neck surgeons. Level IA nodes are in the midline submental region. IB nodes are in the lateral submandibular region anterior to the posterior margin of the submandibular gland and superior to the inferior margin of the hyoid bone. Level II through IV nodes are the jugular nodes. Level II extends from the skull base to the bottom of the body of the hyoid bone. IIA nodes are posterior to the IB region and anterior to the posterior aspect of the jugular vein. IIB nodes are posterior to the jugular vein. Level III nodes are below the hyoid, above the lower margin of the cricoid cartilage, and anterior to the posterior aspect of the sternocleidomastoid. Level IV nodes are below level III and above the clavicle. Level V nodes are posterior to the sternocleidomastoid.
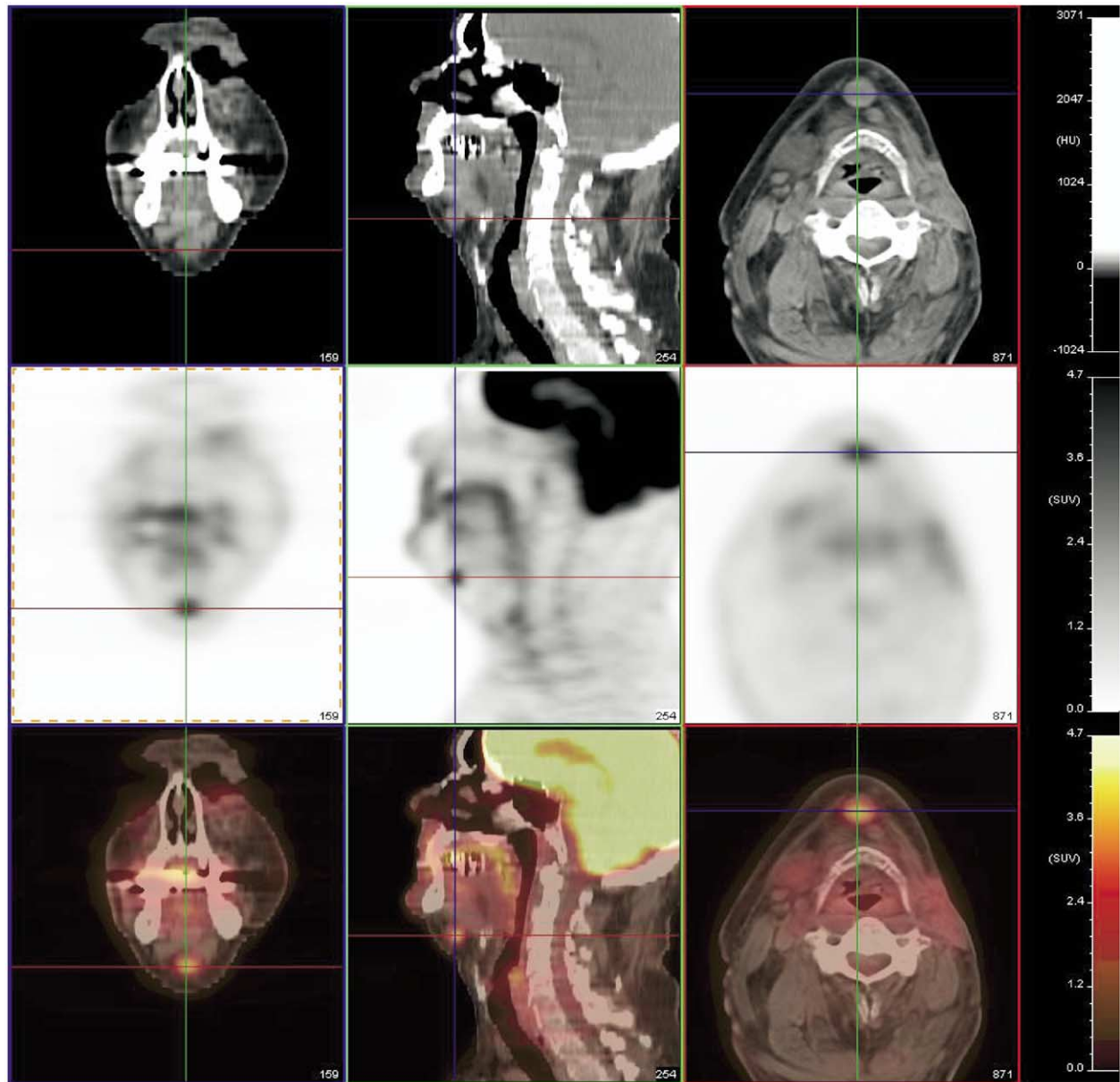
Figure 24 Level IA node in the midline inferior to the mandible. These are most commonly associated with cancer of the tongue or floor of mouth.
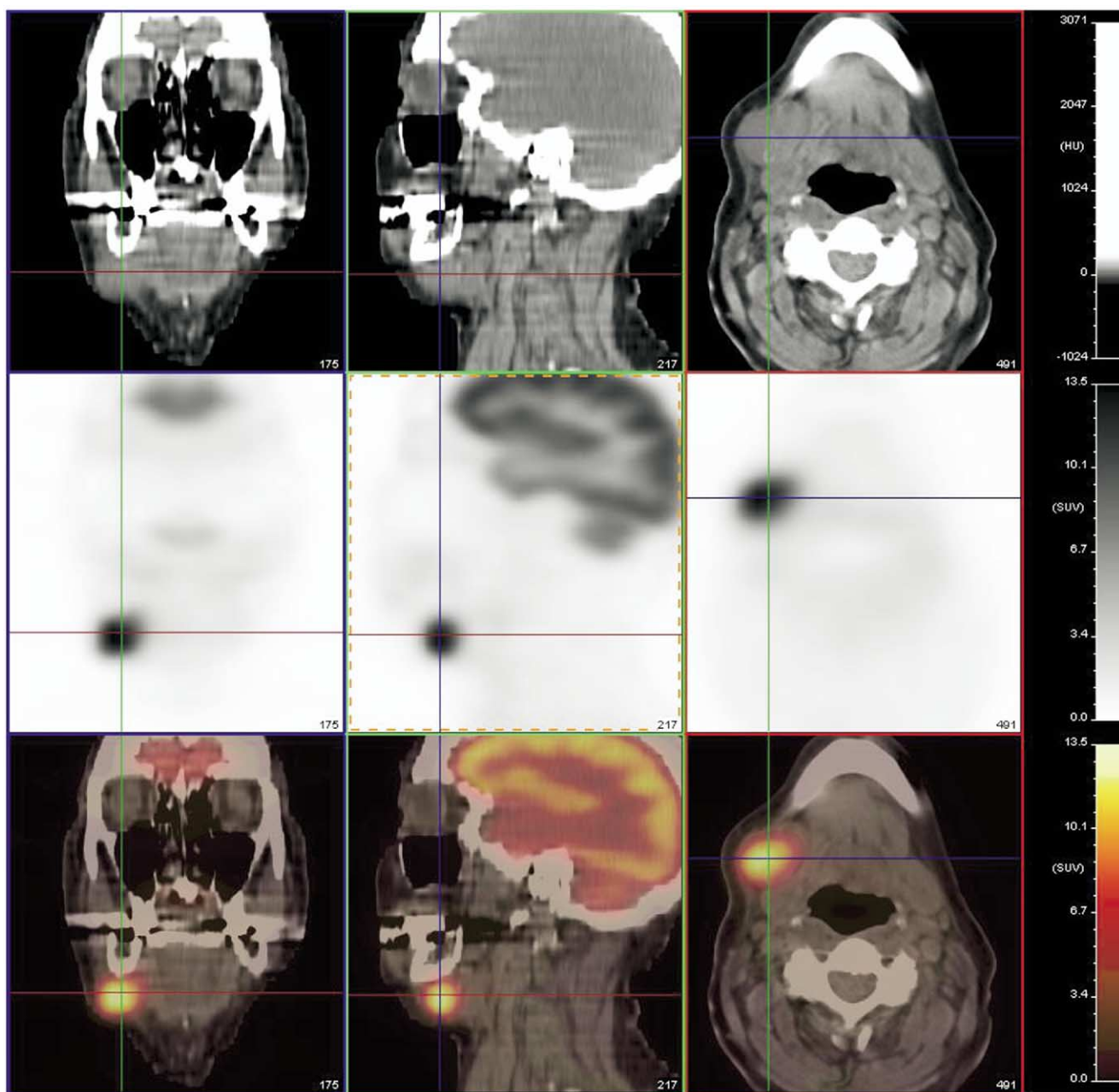
Figure 25 Level IB node, in the lateral submandibular region, anterior to the submandibular salivary gland. The submandibular gland can be seen on the CT images immediately posterior to the node.
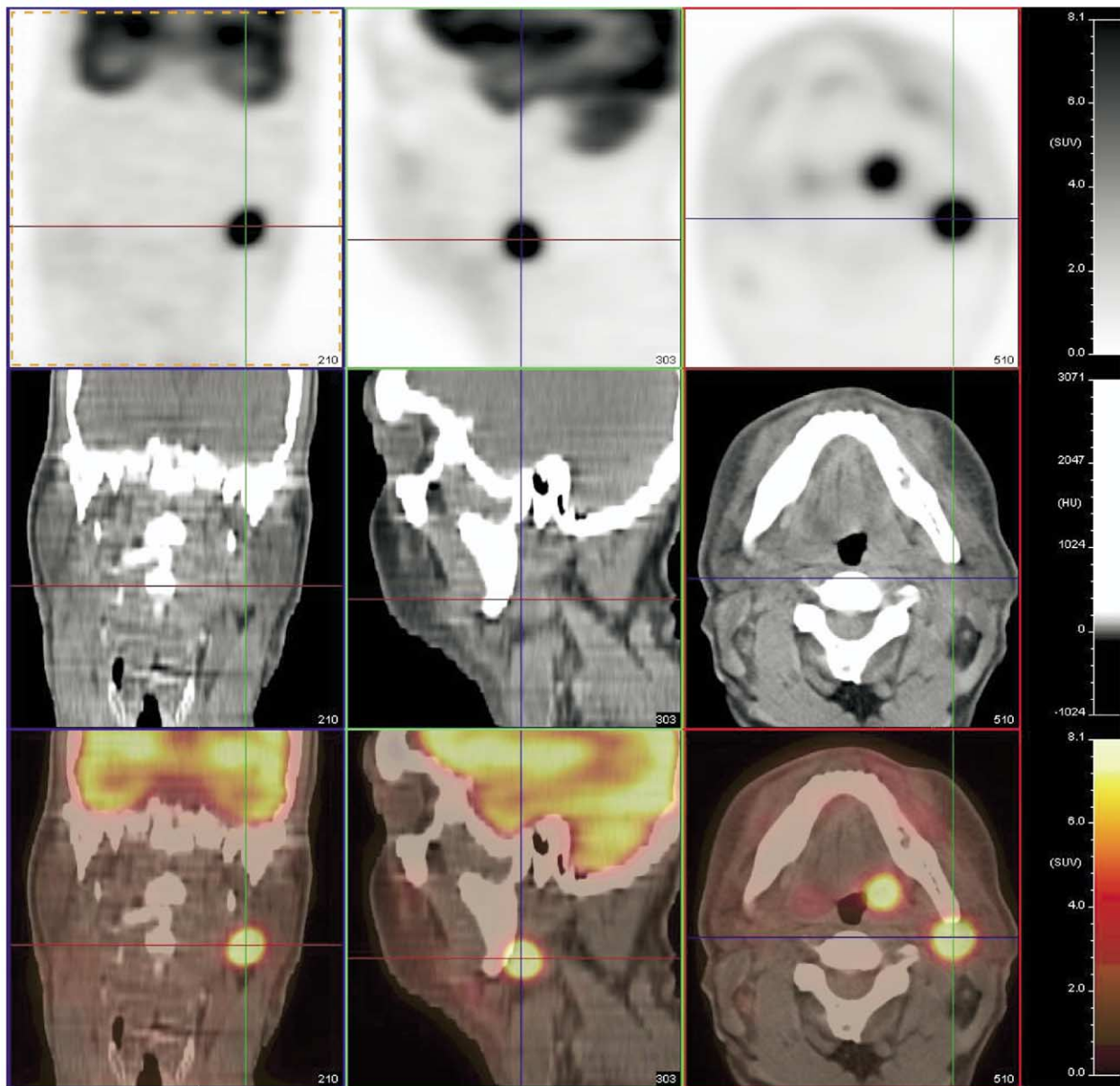
Figure 26 Level IIA node in a patient with a right lingual tonsillar carcinoma. This is the most common node associated with carcinoma of the tonsils. It is also know as the jugulodigastic node. It is located just inferior and posterior to the angle of the mandible.
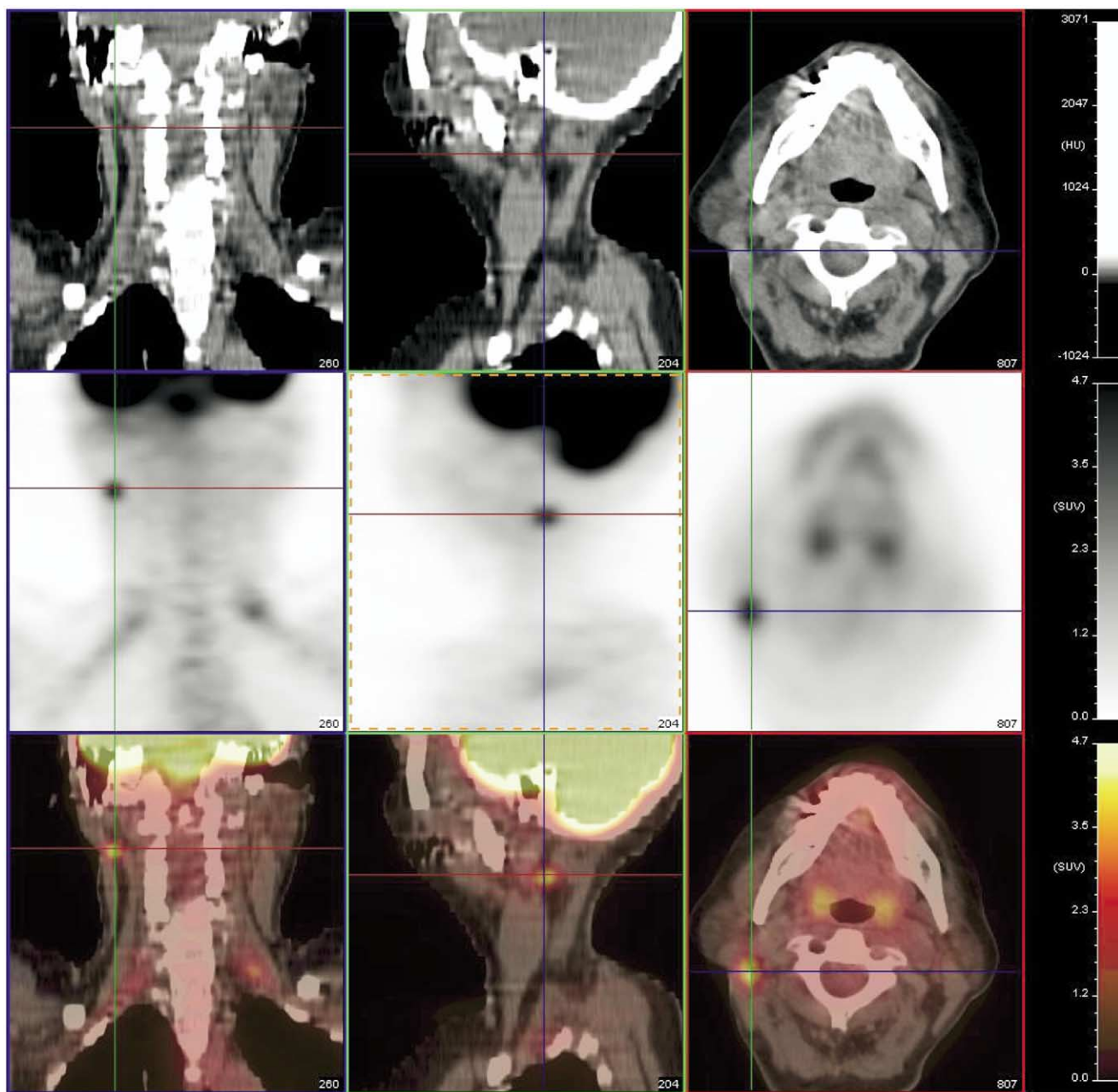
Figure 27 Level IIB node. It is located considerably more posterior than the IIA node seen in Figure 26. On the coronal images it can be seen beneath the sternocleidomastoid muscle. This is less apparent on the other views, although when the images are scrolled at the computer console, it is easy to demonstrate its location beneath the sternocleidomastoid muscle.
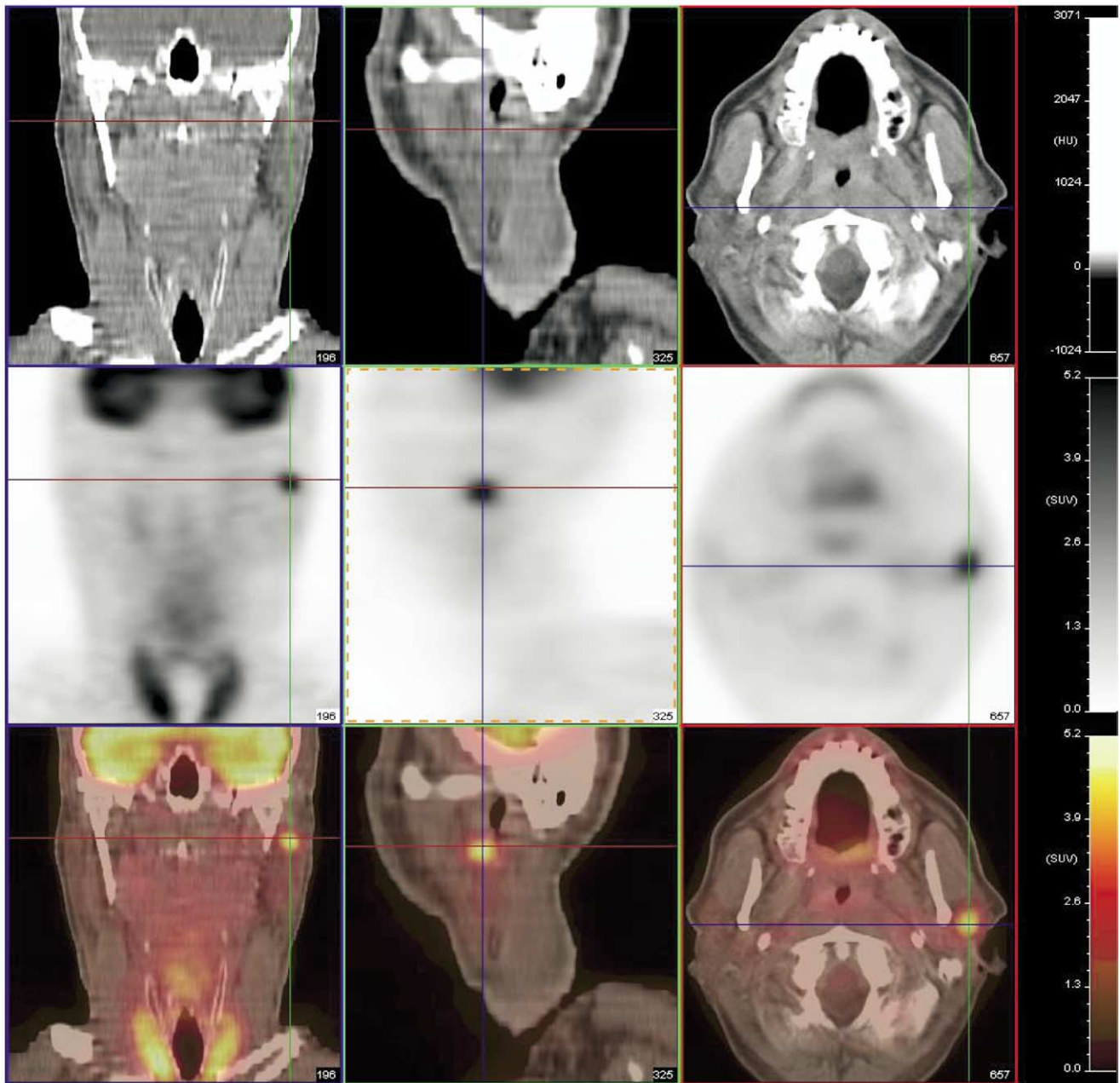
Figure 28 Intraparotid lymph node. Intraparotid nodes, as well as other deep sites such as retropharyngeal nodes, are outside of the general level classification. This node might be identified as a level IIB node; however, it is much more appropriate and useful to the surgeon to identify it as an intraparotid node. This identification requires careful examination of the images, often with magnification.
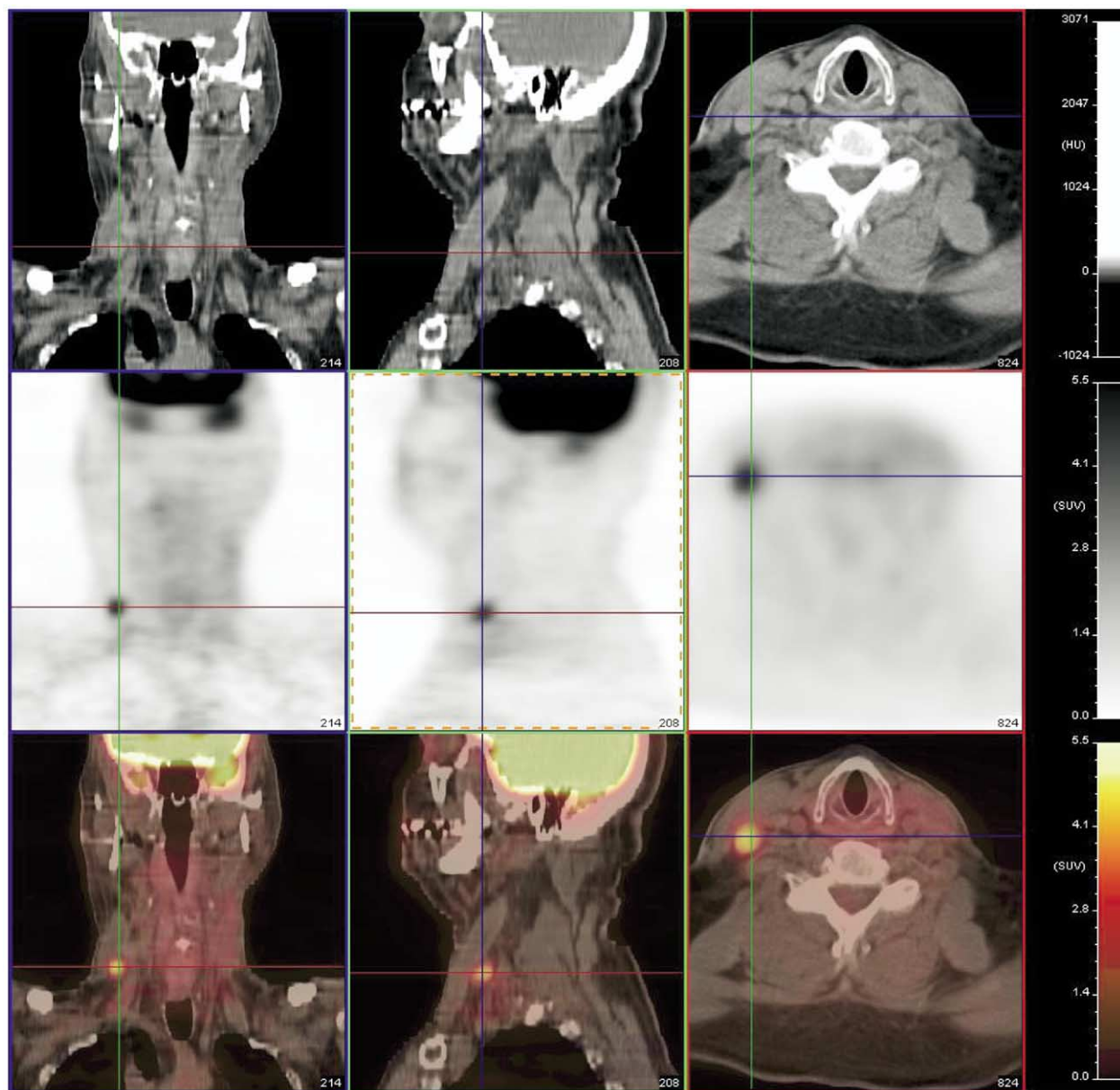
Figure 29 Level III lymph node. This node is at the level of the thyroid cartilage, well above the lower margin of the cricoid cartilage. On the sagittal CT images the node appears to be posterior to the sternocleidomastoid muscle. It is apparent by scrolling the sagittal images at the computer console and on the transaxial images that it is actually beneath the sternocleidomastoid muscle.
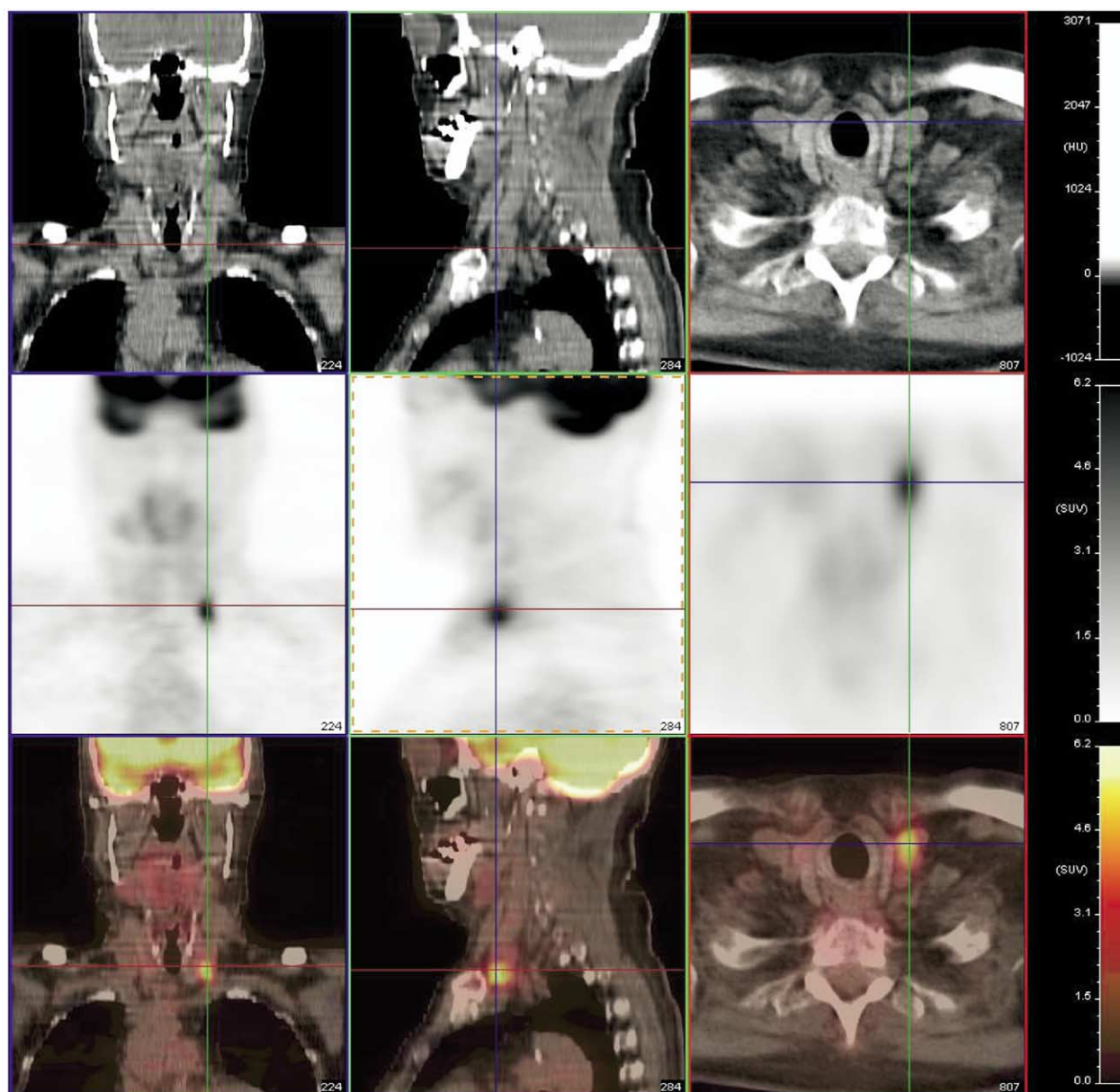
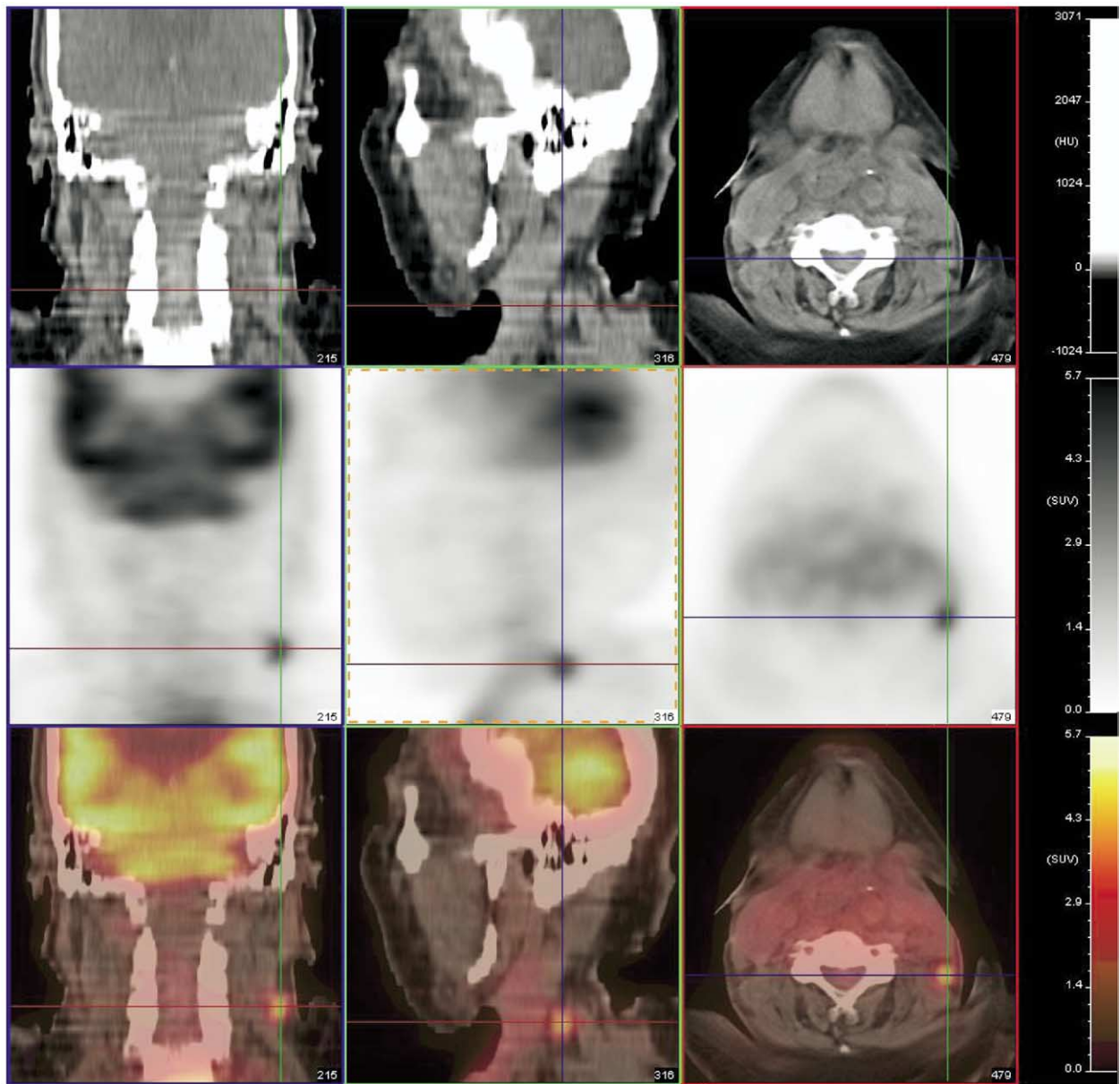**Figure 30** Level IV lymph node, just superior to the left clavicle.

Figure 31 VA lymph node. It is clearly posterior to the sternocleidomastoid muscle, which is observed very well on the sagittal images.
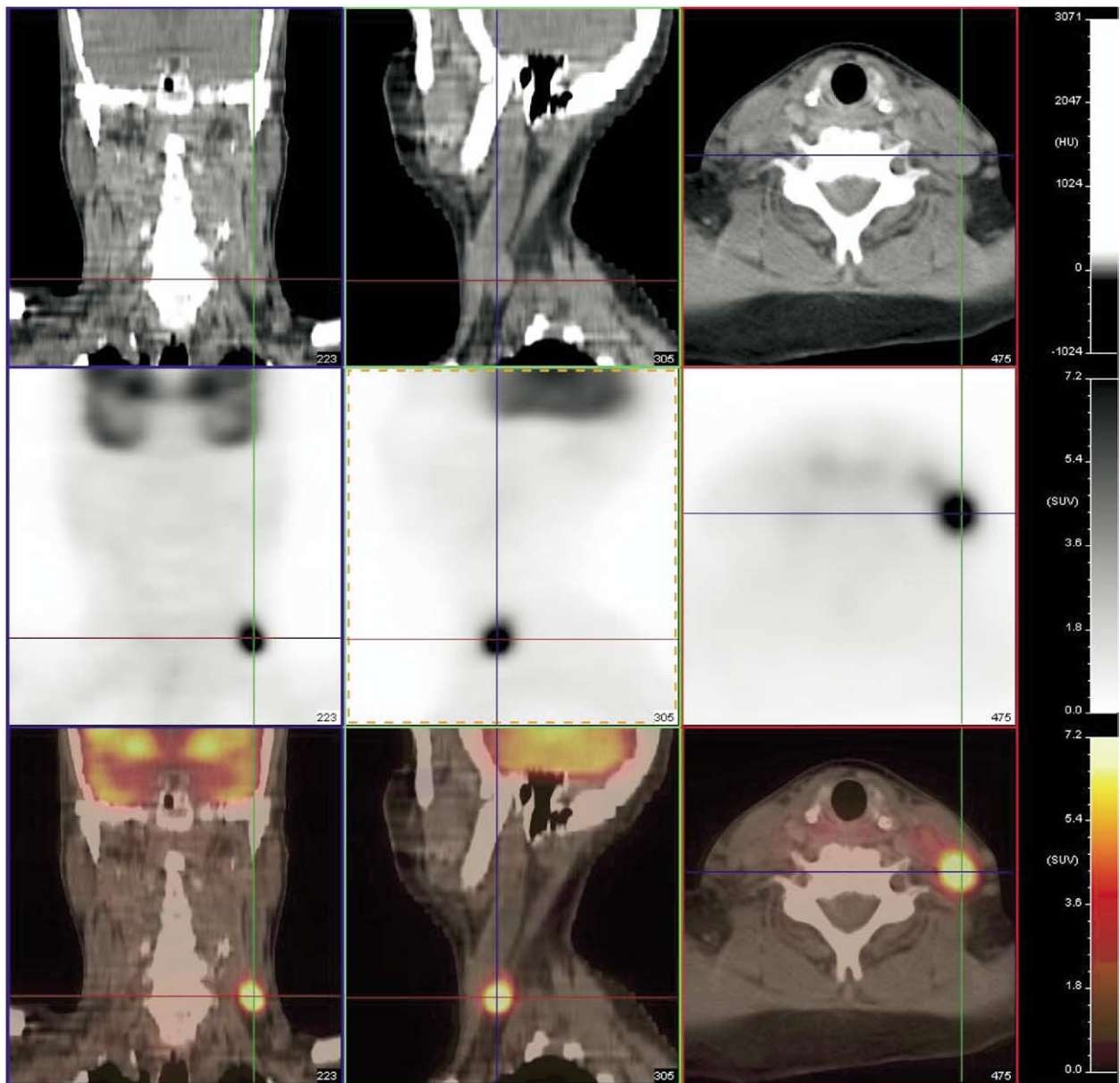
Figure 32 VB lymph node. As with the VA node, it is clearly posterior to the sternocleidomastoid muscle, which is observed very well on the sagittal images.